







Cite this: *Sustainable Energy Fuels*,  
2025, 9, 4375

# Comparative life cycle assessment of lead-free halide perovskite composites/polymer for piezoelectric energy harvesting†

Iván P. Franco, <sup>a</sup> Monica Morales-Masis, <sup>b</sup> Iván Mora-Seró <sup>\*a</sup>  
and Rosario Vidal <sup>\*a</sup>

Lead zirconate titanate (PZT) is one of the most widely used piezoelectric materials due to its excellent performance. However, its lead content raises serious environmental and health concerns, prompting the search for more sustainable alternatives. In this work, we explore whether a lead-free composite based on the halide perovskite  $\text{FASnI}_3$  embedded in a polyvinylidene fluoride (PVDF) matrix could serve as a viable substitute for PZT in piezoelectric energy harvesting applications. To assess this potential, we conduct a comparative life cycle assessment (LCA) of both materials in thin-film device configurations, following a cradle-to-grave approach. The analysis includes the environmental impacts of raw material extraction, manufacturing, potential energy recovery during use, end-of-life treatments, and accidental release scenarios. The results show that PZT-based devices have consistently higher environmental impacts across all life cycle stages, mainly due to the high energy requirements for their synthesis and thin-film deposition, as well as the use of lead. In contrast, the  $\text{FASnI}_3$ -PVDF composite benefits from low-temperature processing and the absence of lead, resulting in significantly lower impacts during manufacturing and the use phase. This study offers a first comparative insight into the environmental trade-offs of substituting PZT with halide perovskite-based composites, contributing to the identification of more sustainable piezoelectric solutions.

Received 20th May 2025  
Accepted 2nd July 2025

DOI: 10.1039/d5se00717h

rsc.li/sustainable-energy

## 1. Introduction

The realm of piezoelectric materials has intrigued the scientific community since the important discovery in 1880 made by the Curie brothers.<sup>1</sup> These materials are distinguished by their unique ability to interconvert mechanical energy and electrical energy. The piezoelectric effect encompasses two primary phenomena: the direct and indirect effects. The direct effect generates electrical charge when mechanical stress is applied to a piezoelectric material, enabling applications like generators,<sup>2</sup> sensors,<sup>3</sup> accelerometers,<sup>4</sup> and medical ultrasound devices.<sup>5</sup> The indirect effect causes mechanical deformation when an electric field is applied, and is utilized in a variety of applications such as actuators, piezoelectric motors,<sup>6</sup> and precision movement devices.<sup>7</sup>

This technology has been extensively studied as a promising alternative to traditional batteries in specific applications that are exposed to consistent mechanical load. One of the most

popular ideas is to implement these devices in roadways. They can be installed in all types of roads, operate independently of weather conditions, be designed in a wide range of sizes and shapes, and have no adverse effects on the lifespan of the pavement.<sup>8,9</sup> Piezoelectric energy harvesters (PEHs) offer a sustainable solution to power electronic devices, especially in scenarios where battery replacement is impractical, costly, or environmentally detrimental. This capability is particularly relevant in applications such as structural health monitoring, remote sensors, and wearable electronics,<sup>10</sup> where reliable and maintenance-free energy sources are crucial.

As evidenced by their widespread application in numerous electronic devices, piezoelectric materials play an important role in a variety of technologies. The global piezoelectric devices market, valued at USD 29.23 billion in 2021, is projected to grow at a compound annual growth rate (CAGR) of 5.7% over the forecast period. Key drivers of this market expansion include the demand for miniaturized electronic devices such as smart-phones, wearables, and IoT products. These applications require compact and efficient components for sensing, actuation, and energy harvesting.<sup>11</sup>

Lead-zirconate-titanate (PZT) ceramics have long been at the forefront of piezoelectric technology, renowned for their exceptional ferroelectric and piezoelectric properties. These materials exhibit high spontaneous polarization, remarkable

<sup>a</sup>Institute of Advanced Materials (INAM), Universitat Jaume I, Av. Sos Baynat, s/n, Castelló de la Plana 12071, Spain. E-mail: vidal@uji.es

<sup>b</sup>MESA+ Institute for Nanotechnology, University of Twente, Enschede 7500 AE, The Netherlands

† Electronic supplementary information (ESI) available. See DOI: <https://doi.org/10.1039/d5se00717h>



dielectric permittivity, and outstanding piezoelectric coefficients, reaching up to  $1000 \text{ pm V}^{-1}$  in bulk form and exceeding  $300 \text{ pm V}^{-1}$  in thin films.<sup>12–14</sup> Introduced by Hans Jaffe in 1954,<sup>14</sup> its versatility allows for the synthesis of a wide range of materials with diverse properties by forming solid solutions over a broad range of Zr:Ti ratios. This adaptability makes PZT a crucial material in numerous applications, offering tailored solutions to meet specific technological needs. PZT is typically synthesized through a solid-state reaction involving the mixing of lead oxide (PbO), zirconium dioxide ( $\text{ZrO}_2$ ), and titanium dioxide ( $\text{TiO}_2$ ). These precursor powders are thoroughly mixed and then calcined at high temperatures, usually ranging from  $800^\circ\text{C}$  to  $900^\circ\text{C}$ , to promote the formation of the perovskite phase. Following calcination, the resulting powder is milled, pressed into the desired shapes, and subsequently sintered at even higher temperatures over  $1000^\circ\text{C}$ .<sup>15</sup> This sintering process enhances the material's densification and crystallinity, which are crucial for achieving the desired piezoelectric properties of PZT. However, it also significantly increases the energy required for its production. PZT is also widely fabricated in thin film form, for which solid targets composed of sintered PbO,  $\text{ZrO}_2$  and  $\text{TiO}_2$  as described above, are used as source materials for pulsed laser deposition (PLD) or sputtering deposition of PZT thin films. To achieve high quality films, substrate temperatures above  $600^\circ\text{C}$  are also required.<sup>16–18</sup> The main challenge with current PZT materials is their lead content. In the European Union, directives such as the Restriction of Hazardous Substances (RoHS),<sup>19</sup> which limits the use of hazardous substances like lead, and the Waste Electrical and Electronic Equipment (WEEE) Directive,<sup>20</sup> with its stringent recycling requirements, are driving the search for lead-free alternatives in piezoelectric devices. Although RoHS generally restricts the use of lead, certain exemptions still apply for specific functional materials. Notably, exemption 7(c)-IV, which allowed the use of lead in PZT-based dielectric ceramic materials for capacitors that are part of integrated circuits or discrete semiconductors, expired on 21 July 2024. In addition, exemption 7(c)-I, which permits the use of lead in glass or ceramic materials other than dielectric ceramics, such as in piezoelectric devices, is set to expire on 31 December 2027. This latter exemption has been extended due to the current lack of viable high-performance alternatives, acknowledging that the replacement of PZT remains technologically and economically unfeasible for many applications. These exemptions are subject to periodic review, creating growing regulatory pressure to accelerate the development of sustainable, lead-free piezoelectric materials.<sup>21,22</sup>

Halide perovskites have recently attracted growing interest as potential piezoelectric materials, offering advantages such as low-temperature processability and possibility to present non-centrosymmetric phases that could give rise to piezoelectric properties. The low temperature and simple processing is a notable contrast to conventional oxide perovskites like PZT, which require synthesis and sintering temperatures above  $1000^\circ\text{C}$ .<sup>23–25</sup> Their compatibility with energy-efficient fabrication techniques, such as microwave-assisted synthesis, further highlights their potential by enabling rapid and uniform heating that reduces both processing time and energy

consumption.<sup>26</sup> These characteristics have positioned halide perovskites as promising candidates for piezoelectric applications in fields ranging from energy harvesting to sensors and actuators.<sup>27</sup> Notably, some halide perovskites have demonstrated exceptional piezoelectric performance in single crystal form. In 2017 a hybrid organic-inorganic perovskite, trimethylchloromethylammonium ( $\text{TMCM}$ )- $\text{MnCl}_3$ , was reported exhibiting a piezoelectric coefficient ( $d_{33}$ ) of  $185 \text{ pC N}^{-1}$ .<sup>28</sup> Similarly, in 2020, vacancy-ordered double perovskite incorporating tin,  $\text{TMCM}_2\text{SnCl}_6$  achieved a  $d_{33}$  of  $137 \text{ pC N}^{-1}$ .<sup>29</sup> To extend these achievements beyond single crystal formats, recent research has shifted toward the development of halide perovskite-based composites. An effective trade-off between mechanical flexibility and functional performance has been demonstrated by piezoelectric composites that embed ceramic materials within polymer matrices.<sup>30–32</sup> These systems often outperform single-phase materials, offering enhanced electro-mechanical coupling, lower electrical impedance, and improved mode stability while remaining cost-effective and suitable for flexible applications. By combining the functional properties of halide perovskites with the mechanical flexibility and chemical resilience of polymers, these composites aim to achieve enhanced performance, improved stability, and easier processability. In particular, the integration of halide perovskites with polyvinylidene fluoride (PVDF), a piezoelectric polymer known for its flexibility and high piezoelectric response, has shown great promise.<sup>33</sup>

The  $\text{FASnI}_3$ -PVDF composite, for instance, exemplifies this approach. While  $\text{FASnI}_3$  provides the semiconducting and piezoelectric functionality, PVDF contributes mechanical robustness and environmental compatibility. This synergy has led to a composite material capable of delivering strong piezoelectric performance ( $d_{33} = 73 \text{ pC N}^{-1}$ )<sup>34</sup> at relatively low processing temperatures ( $\sim 70^\circ\text{C}$  for the active layer), making it a compelling lead-free alternative to PZT for thin-film, flexible piezoelectric devices. Thin-film piezoelectrics have a wide range of potential applications, including lightweight, flexible substrates, and integration into wearable or miniaturized IoT devices.<sup>35–37</sup>

Conducting a life cycle assessment (LCA) is crucial for evaluating the environmental impacts of piezoelectric materials throughout their entire lifecycle, from raw material extraction to end-of-life disposal. These assessments are necessary to justify the replacement of one material with another that is environmentally superior. The pioneering work by Ibn-Mohammed between 2016 and 2018 was among the first to explore the environmental profiles of lead-free alternatives like potassium sodium niobate (KNN) and sodium bismuth titanate (NBT), finding that these materials offer no clear environmental advantage over PZT.<sup>38,39</sup> He also contributed to a 2019 paper that delves into the advantages and the need for applying LCA analysis to ceramic materials.<sup>40</sup> Hazeri's studies in 2017 and 2022 focused on energy harvesting in pneumatic tires, comparing the environmental impact of piezoelectric tires with conventional ones.<sup>41,42</sup> Further advancements were published in 2024, continuing the exploration of the environmental impacts of KNN piezoelectrics. This study considered material density



and concluded that KNN has lower environmental impacts, but also highlighted the need for more efficient extraction and purification methods for  $\text{Nb}_2\text{O}_5$  to reduce energy consumption and waste emissions.<sup>43</sup> The number of publications on the piezoelectric properties of halide perovskites has increased significantly in recent years,<sup>44</sup> and there were also 155 active patents for KNN-based piezoelectric ceramics between 2017 and 2022.<sup>43</sup> However, despite this growing interest, only these few studies have focused on conducting LCAs to validate the environmental benefits of these emerging materials.

This research aims to explore environmentally sustainable alternatives to conventional lead-based piezoelectrics by applying a life cycle assessment (LCA) methodology. As a case study, we evaluate a lead-free composite system consisting of the halide perovskite  $\text{FASnI}_3$  embedded in a PVDF matrix. While the analysis is limited to this specific configuration, it serves as a starting point for understanding the broader sustainability implications of emerging lead-free piezoelectric materials. The assessment follows a cradle-to-grave approach, including manufacturing impacts, energy harvesting performance during use, and end-of-life considerations. By focusing on a realistic device architecture, the study highlights key environmental trade-offs and potential benefits associated with moving away from traditional PZT ceramics, while acknowledging the stability challenges of  $\text{FASnI}_3$  and the environmental burden of PVDF. These findings contribute to the ongoing search for safer and more sustainable piezoelectric technologies for energy harvesting.

## 2. Methodology

The LCA methodology employed adheres to the protocols established by the International Organization for Standardization, specifically the guidelines outlined in ISO-EN 14040 (ref. 45) and ISO-EN 14044.<sup>46</sup> According to these standards, LCAs are divided into four critical phases: (i) goal and scope definition (ii) inventory analysis (iii) impact assessment and (iv) interpretation phase.

### 2.1. Goal and scope

The primary objective of this study was to perform a comparative LCA of two distinct piezoelectric materials: the conventional lead zirconate titanate (PZT) ceramics and the novel lead-free hybrid perovskite, specifically formamidinium tin iodide ( $\text{FASnI}_3$ ) incorporated into a PVDF matrix.

The system boundary for the LCA of piezoelectric materials spans from cradle-to-grave, encompassing cradle-to-gate, use phase, and end-of-life, see Fig. 1. In the cradle-to-gate study, both production processes and raw materials preparation for the piezoelectric materials were evaluated. An analysis of the industrial-scale process was performed, assuming finished products of piezoelectric thin films. Various compositions of PZT were selected, assuming the same manufacturing system for all of them, with changes mainly in the quantities of materials precursors used in this process. In the use phase, the devices are applied in energy harvesting scenarios, generating

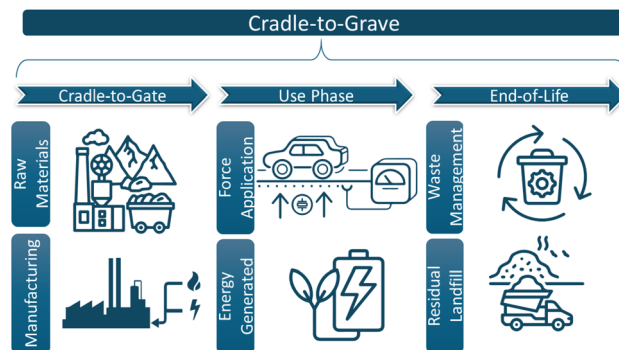


Fig. 1 System boundary of the LCA for piezoelectric materials, covering cradle-to-gate (raw materials and manufacturing), use phase (energy harvesting), and end-of-life (waste management and disposal).

energy in response to mechanical stress. One notable advantage of piezoelectric materials is their ability to replace batteries and operate autonomously throughout their lifespan. This fact eliminates the need for periodic battery replacements and is particularly beneficial in environments where replacing batteries may pose significant challenges due to complexity. Additionally, Ibn-Mohammed has recently emphasized the importance of performing accident analysis alongside a conventional LCA to assess the environmental impacts of unforeseen events.<sup>47</sup> In this study, such an accident scenario was considered, assuming the device breaks and disperses all the piezoelectric material onto the ground. This perspective complements the cradle-to-grave analysis by accounting for potential risks during the use phase.<sup>47</sup>

The study on end-of-life scenarios employed the model for waste-specific and regionalized models for residual material landfills and slag compartments published by Gabor Doka in the 2023 version.<sup>48</sup> It has been assumed that the materials are deposited in a residual material landfill. This system boundary assessment enables a complete cradle-to-grave analysis, offering a clear understanding of the lifecycle impacts. It facilitates a meaningful comparison between traditional lead-based piezoelectrics and emerging lead-free perovskites.

The scarce literature revealed a diversity in the choice of functional units, ranging from specific components, such as a wheel in piezoelectric studies related to vehicular applications,<sup>41,42</sup> to mass-based units like kilograms<sup>38,39,49</sup> or per volume in  $\text{m}^3$ .<sup>43</sup> However, given the focus of this study on materials with varying densities and their application in energy harvesting, adopting area, measured in square meters ( $\text{m}^2$ ), as the functional unit emerged as a more pragmatic approach. This decision is particularly rational for piezoelectric materials used in thin films, as it allows for the consideration of the contact area where force is applied, enabling a more precise assessment of their performance in energy harvesting applications. Energy harvesting is another key parameter in evaluating piezoelectric performance; however, it is highly dependent on factors such as the operating frequency of the device and the applied pressure. To account for this energy in the analysis, this study evaluates energy harvesting under standardized conditions, specifically at



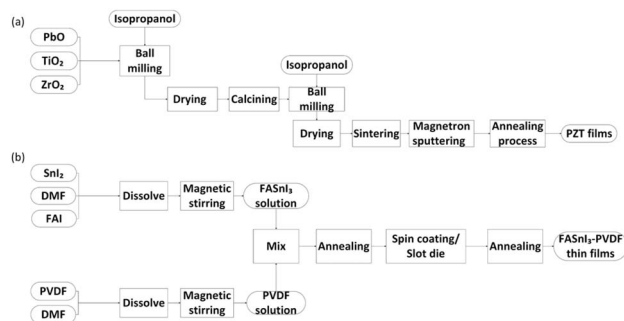


Fig. 2 Flowcharts of the manufacturing process of (a) typical PZT piezoelectrical ceramic deposited in thin films by RF-magnetron sputtering and (b) FASnI<sub>3</sub>-PVDF perovskite deposited in thin films by spin coating/slot-die.

a frequency of 20 Hz and applied pressures of 10 MPa and 100 MPa.

Fig. 2a illustrates the intricate process involved in the fabrication of traditional PZT thin films. The procedure starts with precision batch weighing of PbO, TiO<sub>2</sub>, and ZrO<sub>2</sub>. These components are then subjected to ball milling in the presence of isopropanol, forming a homogenous mixture. The resulting slurry is dried and subjected to a calcination process at elevated temperatures to achieve the desired crystalline structure. A subsequent round of ball milling, followed by another drying phase, prepares the material for sintering at an elevated temperature of 1000 °C. The sintered material is then deposited onto a substrate heated to 600 °C using magnetron sputtering to produce PZT thin films of the desired thickness, in this case 800 nm for easy comparison with the reported FASnI<sub>3</sub>-PVDF thickness. A final annealing step is employed to enhance the piezoelectric and structural properties of the films, optimizing them for their intended applications.<sup>38</sup>

The synthesis process of FASnI<sub>3</sub>-PVDF perovskite thin films, see Fig. 2b, starts with the dissolution of tin iodide (SnI<sub>2</sub>) and formamidinium iodide (FAI) in dimethylformamide (DMF). This mixture is then subjected to magnetic stirring at ambient conditions to ensure the formation of a homogenous FASnI<sub>3</sub> precursor solution. Simultaneously, PVDF is dissolved in DMF and agitated magnetically at a controlled temperature of 60 °C to obtain a stable solution. These two solutions are carefully blended in a 0.5 : 0.5 volume ratio and subsequently annealed at 70 °C to promote the formation of the perovskite structure. The annealed mixture is spin-coated onto a pre-prepared poly(3,4-ethylenedioxythiophene) polystyrene sulfonate (PEDOT:PSS) film for a precise duration of one minute, laying the foundation for the 800 nm thick perovskite thin film. To optimize the film's performance, a final annealing process to 70 °C is implemented. This step helps to refine the microstructure and bolster the intrinsic piezoelectric and electronic characteristics of the film, ensuring that its properties are not only enhanced but also consistent.<sup>34</sup>

In Table 1, the different types of piezoelectric materials analyzed are documented alongside their  $d_{33}$  value. Efforts were made to identify materials with similar piezoelectric

Table 1 Summary of piezoelectric materials with their piezoelectric coefficients  $d_{33}$  values (pC N<sup>-1</sup>) and corresponding energy harvesting figures of merit (FoM) used for comparative performance evaluation

Piezoelectric product	$d_{33}$ (pC N <sup>-1</sup> )	FoM $\left(\frac{d_{33}^2}{\epsilon_{33}}\right)$
FASnI <sub>3</sub> -PVDF	73 (ref. 34)	$4.38 \times 10^{-10}$
PZT	75 (ref. 50)	$6.69 \times 10^{-13}$
PZT-5H	650 (ref. 53)	$5.30 \times 10^{-11}$
PZT-5A	390 (ref. 53)	$1.91 \times 10^{-11}$
PZT-5J	500 (ref. 53)	$3.14 \times 10^{-11}$

coefficients. For the perovskite FASnI<sub>3</sub>-PVDF, a  $d_{33}$  value of 73 pC N<sup>-1</sup> was determined,<sup>34</sup> while for the sputtered PZT ceramic, the  $d_{33}$  value was found to be 75 pC N<sup>-1</sup>.<sup>50</sup> This equivalence in  $d_{33}$ , a measure of the material's ability to convert mechanical stress into electrical charge, serves as a critical benchmark for assessing performance under similar operational conditions. It allows for a direct and fair comparison of their efficiency and effectiveness in energy conversion applications. Additionally, to analyze the usage stage, more commercial PZTs were considered to explore how their environmental impacts varies due to their different piezoelectric properties. Specifically, soft PZT materials such as PZT-5H, PZT-5A, and PZT-5J, see Table 1, were compared. They are commonly used as reference materials due to their large transduction coefficient which helps to generate high energy and power densities.<sup>51</sup> These materials outperform hard PZT counterparts under low-frequency off-resonance excitation conditions.<sup>52</sup>

## 2.2. Inventory analyses

Comprehensive inventories for each proposed material were compiled, addressing both laboratory and industrial production scales. The sourcing of raw materials leverages data from the Ecoinvent 3.9 database,<sup>54</sup> with specific deviations and justifications provided where applicable. All inventory tables are in the ESI (see Tables S1–S9).†

For the PZT laboratory case, the inventory of material and energy inputs was modeled based on data provided by Ibn-Mohammed's work (Table S1†).<sup>38</sup> Adjustments were made to increase the amount of PbO (Table S2†) used compared to the initial data, compensating for lead oxide losses due to evaporation at high temperatures during the synthesis of PZT materials.<sup>55</sup> Additionally, isopropanol was introduced as a solvent in the solid-state reaction.<sup>56</sup> At industrial scale, a 95% solvent recirculation rate was assumed, and electricity consumption was calculated using theoretical equations derived from an industrial-scale thermodynamic study conducted by Piccinno.<sup>57</sup> In both laboratory and industrial contexts, sputtering has been identified as one of the most widely used and effective techniques for depositing PZT in thin films.<sup>58</sup> For laboratory-scale sputtering, a material loss of 61% was considered, while for industrial-scale sputtering, losses were assumed to be only 5%, based on the utilization of the entire target material and the implementation of a protective shield to recover residual material.<sup>59</sup>





The lead-free hybrid perovskite system consists of  $\text{FASnI}_3$  embedded in a soft PVDF polymer matrix with a volumetric ratio of 0.5 : 0.5. The quantities for halide perovskite composite synthesis were derived from the study conducted by Pandey (Tables S3 and S4†).<sup>34</sup> Electricity consumption for the spin-coating deposition process was measured at our laboratory using a CIRCUTOR MYeBOX 1500 Network Analyzer, capturing data every second from a Laurell WS-650Lz-23NPPB spin coater.

At an industrial scale, a 95% solvent recirculation rate was also assumed for perovskite deposition. While spin coating is commonly employed in laboratory settings, it is inefficient for large-scale production. The literature highlights several deposition methods suitable for industrial applications. For this study, slot-die coating was selected as the industrial deposition method due to its scalability, cost-effectiveness, and reproducibility. Energy consumption associated with slot-die coating was estimated using a reliable industrial-scale ref. 60.

Li-ion battery cell featuring a nickel manganese cobalt 811 (NMC811) cathode and a silicon-coated graphite-based anode has been utilized for energy study, sourced from Ecoinvent. This cell provides a specific energy capacity of  $0.209 \text{ kWh kg}^{-1}$ . This comparison is significant as piezoelectrics could avoid the use of batteries for certain applications and consequently the impacts of their fabrication, see below.

Some data are not available in the Ecoinvent 3.9 database and have been modeled independently. Details on the modeling approach for these compounds are provided in the ESI.†

### 2.3. Energy harvesting

Energy harvesting refers to the process of capturing and converting ambient energy from the environment into electrical power, which can be used to power small devices. This energy can come from various sources like vibrations, heat, light or radio waves. Piezoelectric materials are key in this process because they generate electricity when they are mechanically stressed. For energy harvesting calculations, it is considered that the piezoelectric material behaves similar to a capacitor in an open-circuit setup. This boundary condition is crucial for designing absorbers and vibration sensors.<sup>64</sup> In Fig. 3, a schematic representation of a typical piezoelectric device for this purpose is shown. The stacked structure for piezoelectric energy harvesters was selected due to its advantages, such as higher output in the  $d_{33}$  mode, suitability for pressure-mode operation, and its capability to withstand high mechanical loads.<sup>62</sup> This structure is composed of an encapsulation layer, which could be made of materials such as polymers or ceramics to protect the internal components. Beneath this is the substrate, which provides mechanical support and stability to the entire device. Two electrodes, a top and a bottom, are positioned around the central piezoelectric film layer.<sup>63–65</sup>

This study focuses on the comparison of the piezoelectric layer, assuming that the other layers remain constant across different materials. By holding these layers constant, we eliminate their influence on the results, allowing for a clearer environmental assessment of the piezoelectric materials being compared.

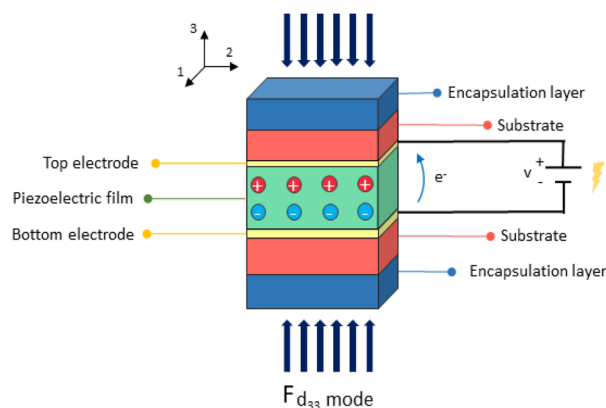


Fig. 3 Schematic diagram of a typical piezoelectric device for energy harvesting, illustrating the encapsulation layer, substrate, and the central piezoelectric film between two electrodes.

By treating the piezoelectric element as a capacitor, we can effectively model and compute the potential energy harvesting capabilities, thereby establishing a fundamental basis for assessing the efficiency and efficacy of these materials in converting mechanical energy into electrical energy.<sup>66</sup> For the open circuit, voltage and current are determined by the following equations:<sup>67</sup>

$$V = \frac{d_{33}}{\epsilon_{33}^T} \cdot h \cdot \sigma \quad (1)$$

$$I = d_{33} \cdot A \cdot \frac{\Delta\sigma}{\Delta t} \quad (2)$$

where  $V$  is the voltage,  $I$  is the current,  $d_{33}$  is the piezoelectric coefficient,  $\epsilon_{33}^T$  is the permittivity at constant stress along the polarization direction,  $h$  is the thickness of the piezoelectric layer,  $\Delta\sigma$  is the stress applied,  $A$  is the area and  $\Delta t$  is the period of time in which the stress is applied.

Energy is computed by considering capacitance and time, taking into account that the energy stored in a capacitor follows the formula  $E = 1/2 CV^2$ . This energy formula can be expressed as follows:<sup>67</sup>

$$E = \frac{1}{2} C \frac{d_{33}^2}{\epsilon_{33}^T} \cdot h^2 \cdot \Delta\sigma^2 \cdot t \quad (3)$$

where  $C$  is the capacitance and can be described as:

$$C = A \cdot \frac{\epsilon_{33}^T}{h} \quad (4)$$

As a result, the energy equation can be written in the following way:<sup>67</sup>

$$E = \frac{1}{2} \frac{d_{33}^2}{\epsilon_{33}^T} \cdot A \cdot h \cdot t \cdot \Delta\sigma^2 \quad (5)$$

Coefficients such as  $d_{33}$  and  $\epsilon_{33}^T$  have been found to generally increase with temperature for both soft and hard PZT samples. Additionally, thermal hysteresis was observed in all the studied material coefficients over the temperature cycle.<sup>68</sup> Additionally,



dielectric losses ( $\tan \delta$ ) at low frequencies were found to be negligible, simplifying the comparison between different materials.<sup>69</sup>

Larger dimensions of the piezoelectric device yield greater energy output. Moreover, increasing the  $d_{33}$  coefficient and the applied force significantly enhances the energy harvested. Therefore, attaining high  $d_{33}$  values and low  $\epsilon_{33}^T$  permeabilities will be crucial for achieving greater energy output. To ensure a fair comparison of the materials, all simulations in this study were performed under identical mechanical and geometric conditions. The same applied pressure, device area, and thickness were used in each case. With these parameters held constant, any variation in energy output can be attributed solely to the intrinsic electromechanical properties of the materials.

Under such conditions, the ratio  $\frac{d_{33}^2}{\epsilon_{33}^T}$  is recognized as a figure of merit (FoM) for energy harvesting applications.<sup>67,70</sup> The corresponding FoM values for the materials considered are summarized in Table 1. A constant ambient temperature will be assumed to ensure consistency and comparability across the case studies. This decision stems from the observed variations in certain piezoelectric parameters with temperature.<sup>71</sup>

We use eqn (5) to represent the NET environmental impacts during the use of piezoelectric devices, considering both the energy produced over a given period and the battery impacts avoided as a result. This metric is crucial for evaluating the energy efficiency and environmental feasibility of these devices, as it provides insights into when the energy invested in their production will be offset.

$$\text{NET} = \text{piezoelectric impacts} - \text{avoided battery impacts} \quad (6)$$

The avoided battery impacts (eqn (7)) were calculated based on the environmental impacts of producing an NMC811 battery, with an energy density of 0.209 kWh kg<sup>-1</sup>, as provided in the Ecoinvent database. Using this energy density and the energy generated by the piezoelectric device over a given period, we determined the equivalent amount of battery production that was avoided.

Avoided battery Impacts

$$= \frac{\frac{1}{2} \cdot \frac{d_{33}^2}{\epsilon_{33}^T} \cdot A \cdot h \cdot t \cdot \Delta \sigma^2}{0.209 \text{ kWh kg}^{-1}} \cdot \text{environmental factor} \quad (7)$$

## 2.4. Environmental impacts

The European Footprint 3.1 (EF 3.1) method (adapted) and the cumulative energy demand (CED) v1.0 LHV, included in the software SimaPro 9.5, were chosen to estimate the environmental impact categories. The selected impact categories, along with their abbreviations, are listed in Table 2. Among these, the categories of acidification, climate change, freshwater ecotoxicity, and cumulative energy demand have been specified in greater detail. They provide a clear and comprehensive comparison of the materials' sustainability profiles by addressing atmospheric impacts (*e.g.*, acidification and climate

**Table 2** Environmental categories with abbreviations and units from the EF 3.1 method used in this study

Impact category	Unit	Abbreviation
Acidification	mol H <sub>eq</sub> <sup>+</sup>	AP
Climate change	kg CO <sub>2 eq</sub>	GW
Ecotoxicity, freshwater	CTUe	EcoT
Particulate matter	Disease inc.	PM
Eutrophication, marine	kg N <sub>eq</sub>	EP-m
Eutrophication, freshwater	kg P <sub>eq</sub>	EP-f
Eutrophication, terrestrial	mol N <sub>eq</sub>	EP-t
Human toxicity, non-cancer	CTUh	HT-nc
Human toxicity, cancer	CTUh	HT-c
Ionising radiation	kBq U-235 <sub>eq</sub>	IR
Land use	Pt	LU
Ozone depletion	kg CFC <sub>11 eq</sub>	OD
Photochemical ozone formation	kg NMVOC <sub>eq</sub>	POP
Resource use, minerals and metals	kg Sb <sub>eq</sub>	RU-m
Water use	m <sup>3</sup> depriv.	WD
Cumulative energy demand	MJ	CED

change), ecosystem-specific effects (*e.g.*, freshwater ecotoxicity), and resource efficiency (*e.g.*, cumulative energy demand).

## 2.5. Data quality and uncertainty

This study included an uncertainty assessment to evaluate the reliability of the LCA results. Key aspects of uncertainty in the inventory data were addressed, including reliability, completeness, temporal and spatial correlation, technological relevance, and measurement errors. For inventory data, see ESI,<sup>†</sup> obtained from the Ecoinvent database, uncertainties were already quantified. Data derived from laboratory experiments and literature were evaluated following the guidelines of the Ecoinvent project, using a pedigree matrix to assign scores from 1 (best) to 5 (worst) for six uncertainty factors (reliability, completeness, temporal correlation, geographical correlation, further technological correlation and sample size). Lognormal distributions were applied to assess data quality, and the scores were converted into uncertainty figures using additional factors expressed as contributions to the geometric standard deviation.<sup>72</sup>

The LCA calculations were performed twice: first using a custom spreadsheet tool in Microsoft Excel and then directly in SimaPro 9.5. Monte Carlo simulations with 1000 iterations were conducted in SimaPro to quantify uncertainties, providing results within a 95% confidence interval for environmental impacts.

## 3. Results and discussion

This section presents the findings of the life cycle analysis (LCA) conducted across different stages and scales. First, the results are discussed for the cradle-to-gate stage, including the environmental impacts at the laboratory scale before and after thin-film deposition, as well as at the industrial scale. Subsequently, the avoided impacts during the use phase are analyzed, with a focus on reducing battery dependency through energy harvesting. Finally, a cradle-to-grave analysis is performed,



incorporating an evaluation of end-of-life impacts and culminating in a comparative assessment of different scenarios.

### 3.1. Environmental impacts from cradle-to-gate

**3.1.1 Laboratory-scale.** The cradle-to-gate analysis was performed in two steps: the pre-deposition stage, focusing on material preparation, and the post-deposition stage, which includes thin film deposition. The initial results, illustrated in Fig. 4a, highlight the significantly higher environmental impacts of PZT compared to the  $\text{FASnI}_3$ -PVDF perovskite composite across multiple categories: acidification, climate change, freshwater ecotoxicity, and cumulative energy demand (CED). Further results for all 15 impact categories are available in the ESI (Table S10†), where it is shown that the impacts of  $\text{FASnI}_3$ -PVDF composite are lower than those of PZT across all categories, often by an order of magnitude.

The manufacturing process of  $\text{FASnI}_3$ -PVDF composite demonstrates a lower environmental footprint, primarily due to its simpler fabrication, which avoids high-temperature treatments and minimizes energy usage. In contrast, PZT production is dominated by the impacts of material inputs, such as lead (Pb), contributing heavily to acidification and ecotoxicity, as well as the energy-intensive processes of electricity and heat

consumption, which drive its contributions to climate change and CED.

These findings align with previous studies, which emphasize that energy consumption during PZT manufacturing is a major driver of environmental impacts, particularly in the climate change and CED categories.<sup>39</sup> Additionally, these results are consistent with the latest environmental assessment on piezoelectric devices, which indicates that the greatest impacts in the manufacturing process arise from raw materials, particularly  $\text{PbO}$ , and electricity consumption.<sup>43</sup> This data indicates, on one hand, that the use of a Pb-free materials has a huge effect in the reduction of environmental impacts of piezoelectric materials input. While alternative methods such as hydrothermal synthesis,<sup>73</sup> co-precipitation<sup>74</sup> or pulsed wire discharge<sup>75</sup> offer potential for lowering sintering temperatures, the heat treatments required for PZT ceramics remain more energy-intensive than those for the  $\text{FASnI}_3$ -PVDF composite.

Fig. 4b illustrates the lab-scale distribution of manufacturing impacts for the  $\text{FASnI}_3$ -PVDF composite across all contributing sources: PVDF emerges as the largest contributor to climate change, while DMF is the dominant factor in cumulative energy demand (CED). At industrial scale, however, the implementation of solvent recovery systems can significantly reduce the energy impact associated with DMF, leaving PVDF as the main

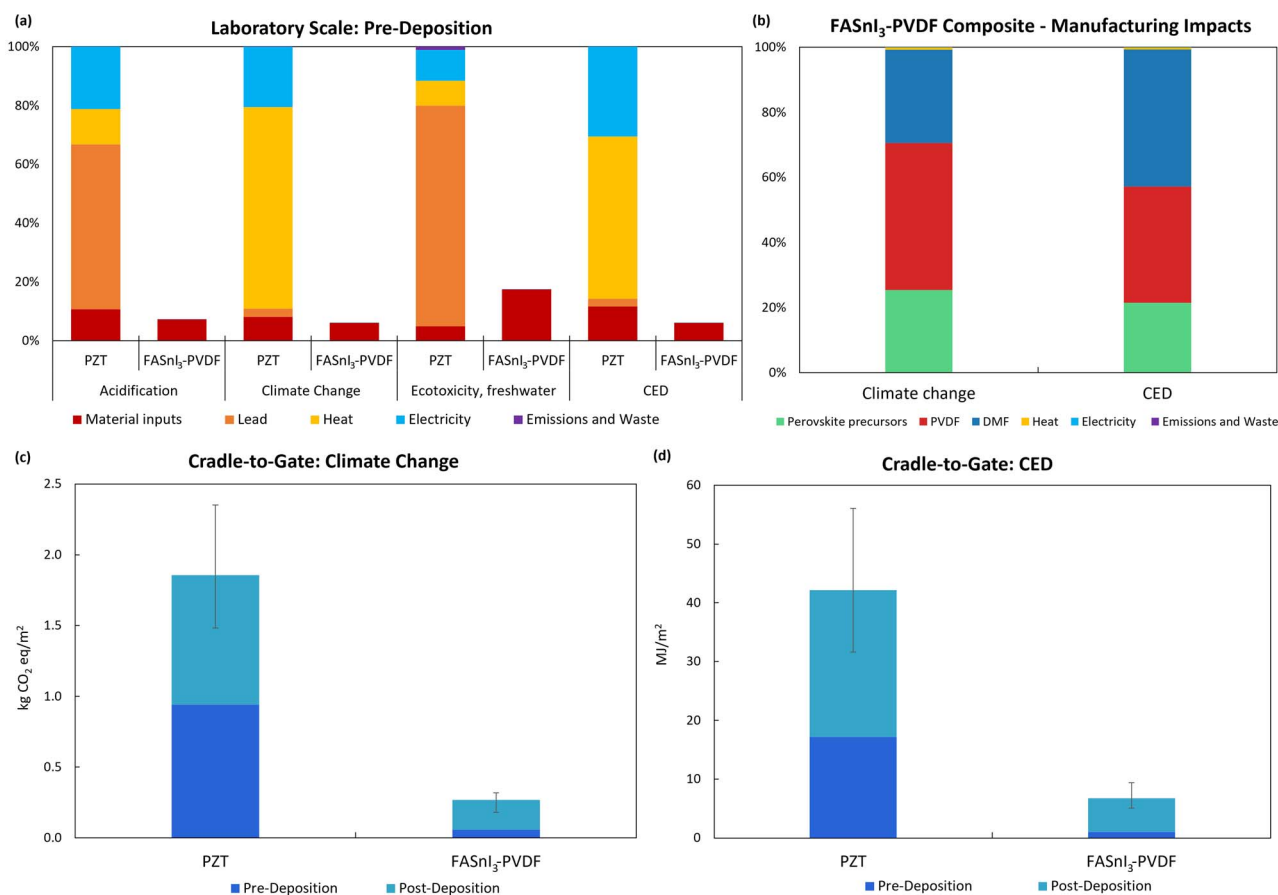


Fig. 4 Comparative cradle-to-gate environmental assessment of PZT and  $\text{FASnI}_3$ -PVDF composite: (a) impacts excluding the deposition stage; (b) contribution of individual sources to the environmental impacts of  $\text{FASnI}_3$ -PVDF; and impacts including the deposition stage for (c) climate change and (d) cumulative energy demand (CED).

environmental hotspot—surpassing even the contributions from the perovskite precursors FAI and  $\text{SnI}_2$ , as well as other process-related emissions and energy use.

When normalized to a one-kilogram functional unit, the cradle-to-gate impacts of the  $\text{FASnI}_3$ -PVDF composite are 24.2 kg  $\text{CO}_2$ -eq per kg for climate change and 443.6 MJ  $\text{kg}^{-1}$  for cumulative energy demand (CED). These values are substantially lower than those reported at laboratory scale for other lead-free ceramic alternatives, such as KNN (248.6 kg  $\text{CO}_2$ -eq per kg and 4123.7 MJ  $\text{kg}^{-1}$ )<sup>38</sup> and NBT (30.4 kg  $\text{CO}_2$ -eq per kg and 447.0 MJ  $\text{kg}^{-1}$ ).<sup>39</sup> Moreover, the implementation of solvent recovery at industrial scale is expected to further reduce these impacts, reinforcing the environmental advantage of  $\text{FASnI}_3$ -PVDF composite over both PZT and other Pb-free piezoelectric materials.

The environmental impacts increase further during the deposition stage, as shown in Fig. 4c and d. For PZT, thin film deposition causes a 97% increase in its climate change impact and a 145% rise in its CED. In contrast, the deposition process

for  $\text{FASnI}_3$ -PVDF composite also contributes to its impacts, but these remain significantly lower overall. This stage is dominated by spin-coating, a widely used laboratory technique with high material losses (up to 99%). As a result, the climate change impact of  $\text{FASnI}_3$ -PVDF composite reaches a mean value of 0.25 kg  $\text{CO}_2$  eq per  $\text{m}^2$ , while its CED is 6.51 MJ  $\text{m}^{-2}$ —reductions of 85.69% and 84.56%, respectively, compared to PZT. The laboratory data underscore that the use of lead-free materials, such as  $\text{FASnI}_3$ -PVDF composite, can substantially reduce the environmental burdens of piezoelectric materials.

**3.1.2 Large-scale industrial production.** The following analysis focuses on the large-scale industrial production of piezoelectric materials, offering a broader perspective on their environmental footprint in commercial applications, see Table S11.† Fig. 5 presents a comparative assessment of the environmental impacts of industrial manufacturing, including both pre-deposition and deposition stages.

The analysis reveals significant differences between the  $\text{FASnI}_3$ -PVDF perovskite composite and PZT ceramics across

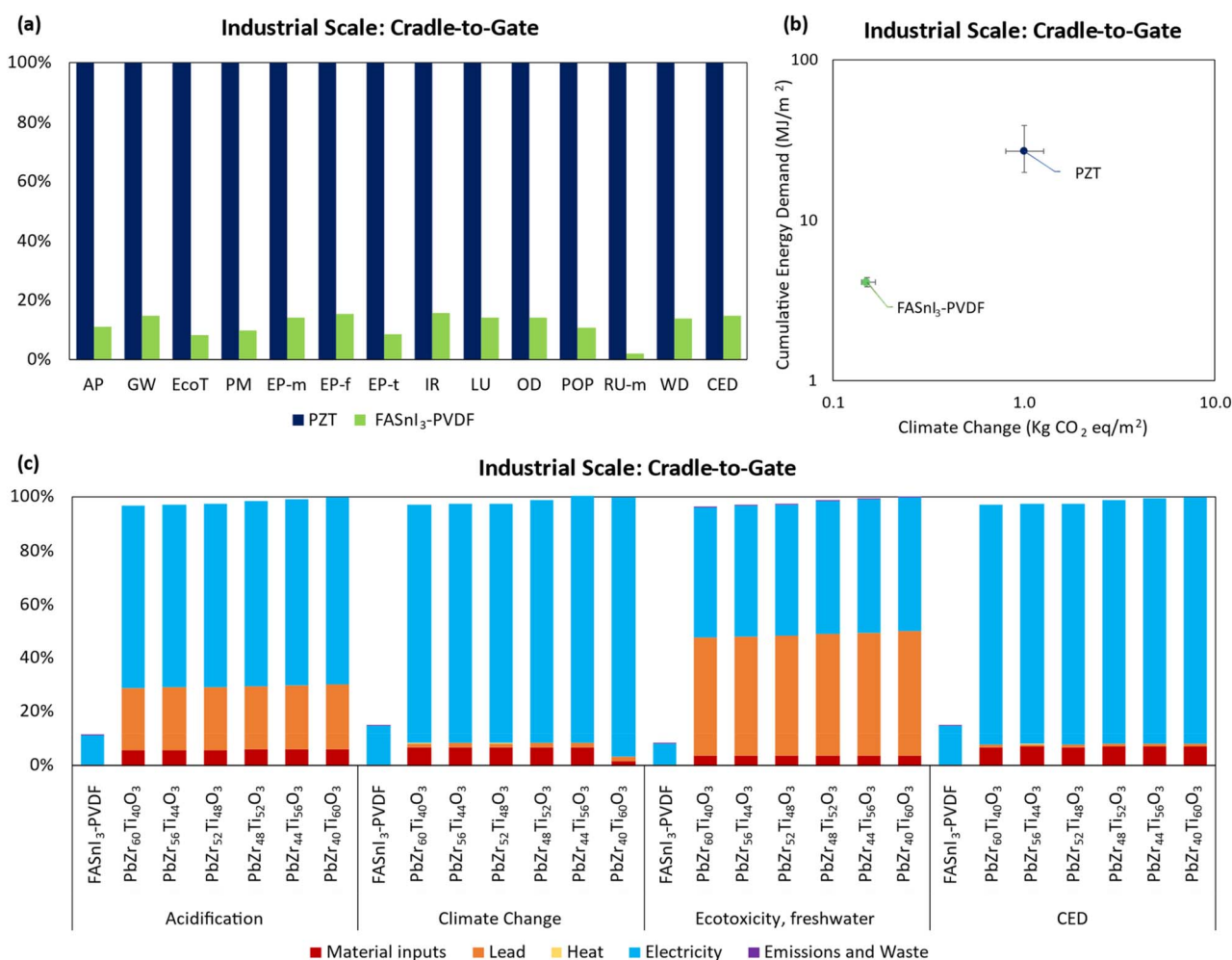


Fig. 5 Comparative environmental assessment impacts of industrial manufacturing for different piezoelectric materials: (a) comparison between PZT and  $\text{FASnI}_3$ -PVDF across different impact categories in cradle-to-gate analysis. (b) Bivariate plot comparing cumulative energy demand (CED) and climate change impacts for PZT and  $\text{FASnI}_3$ -PVDF. The median values are plotted on logarithmic scales with a confidence interval of 95%. (c) Contributions of material inputs, heat, electricity, and air emissions to four selected impact categories—acidification, climate change, ecotoxicity (freshwater), and cumulative energy demand (CED)—including  $\text{FASnI}_3$ -PVDF and multiple PZT compositions.





various environmental categories. As shown in Fig. 5a, PZT consistently exhibits higher impacts, aligning with laboratory-scale observations. For the  $\text{FASnI}_3$ -PVDF composite, industrial-scale slot-die deposition demonstrates a notable advantage over the spin-coating process used in laboratories, dramatically reducing environmental impacts due to significantly lower material losses. Consequently, the industrial-scale environmental impacts of  $\text{FASnI}_3$ -PVDF are markedly lower than those of PZT, further supported by laboratory-scale comparisons (Fig. 4b and c), which highlight the superior environmental performance of the perovskite composite.

Fig. 5b focuses on the cumulative energy demand (CED) and climate change categories, two critical metrics in this study.  $\text{FASnI}_3$ -PVDF exhibits substantially lower values than PZT, primarily due to reduced electricity consumption during industrial manufacturing, leading to lower emissions and potential cost savings. The inclusion of 95% confidence intervals ensures data reliability while accounting for uncertainty in the analysis.

Additionally, Fig. 5c compares various PZT compositions, showing relatively similar environmental impacts across formulations, with a slight increase observed in titanium-rich compositions due to higher density and associated resource demands. In PZT manufacturing, electricity consumption during deposition and the use of raw materials, particularly lead, are the primary contributors to environmental impacts. For acidification and ecotoxicity categories, raw materials account for 30% and 50% of impacts, respectively, with lead playing a dominant role.

From a performance perspective, the largest piezoelectric constant of the PZT ceramics here studied occurs with a Zr/Ti ratio of 52:48, corresponding to a morphotropic phase boundary (MPB) that enhances electromechanical properties. This makes PZT highly effective in applications such as sensors, actuators, and transducers.<sup>55</sup> However, different PZT phases—tetragonal, rhombohedral, and occasionally cubic—exhibit unique electrical and structural properties, which cater to specific applications, including high-temperature sensors, MEMS devices, and ferroelectric memory.<sup>76,77</sup>

Despite its technical advantages, PZT's inherent reliance on lead and higher needs of electrical power contributes significantly to its environmental burden, as shown in Fig. 5c. Addressing these challenges requires transitioning toward lead-free materials with less fabrication power demands, such as  $\text{FASnI}_3$ -PVDF halide perovskite composite. The industrial-scale optimization of the  $\text{FASnI}_3$ -PVDF composite manufacturing process underscores its potential as a safer and more sustainable alternative, offering significant reductions in environmental impacts. By minimizing energy usage and material losses, this composite enables simpler, greener production while maintaining strong performance as a piezoelectric material.

### 3.2. Environmental impacts during use phase

**3.2.1 Avoided impacts from energy harvesting.** By taking into account the avoided impact associated with battery

manufacturing (eqn (6) and (7)), we can calculate the number of cycles needed for piezoelectrics to emerge as a more environmentally sustainable alternative. This is especially relevant in scenarios where energy can be harvested from ambient vibrations and pressures.

In the context of piezoelectric energy harvesting, it is more meaningful to analyze device performance in terms of cycles rather than operational time, given the wide range of frequencies at which these devices can operate. Higher operating frequencies enable more energy generation in less time but also shorten the device's lifespan due to increased mechanical stress. To provide a practical benchmark, a reference frequency of 20 Hz was selected, as it yielded the best performance for the  $\text{FASnI}_3$ -PVDF composite studied. This aligns with typical applications in literature, where many piezoelectric harvesters are designed to operate within low-frequency ranges (0–100 Hz), commonly targeting vibrations from human motion (2–5 Hz),<sup>78</sup> road traffic (3–10 Hz at 30–100 km h<sup>-1</sup>),<sup>79</sup> and household appliances such as refrigerators or air conditioners (25–100 Hz).<sup>80</sup> It is important to emphasize the importance of resonance frequency, where energy output is maximized. Aligning this frequency with the target range can be achieved through design strategies such as modifying geometric dimensions, adding mass, or utilizing flexible materials. Frequency tuning mechanisms and multi-modal designs further enhance efficiency, particularly in environments with variable or low-frequency vibrations.

The pressure exerted on piezoelectric materials plays a crucial role in determining both the amount of energy generated and the durability of the device over multiple cycles. Most studies on piezoelectric energy harvesters focus on pressure ranges between 0.1 and 10 MPa, commonly associated with applications such as human motions (*e.g.*, hand movements<sup>81</sup> or walking), tire pressures from cars and trucks,<sup>82,83</sup> or energy harvesting from machine vibrations. However, PZT-based devices are capable of withstanding pressures exceeding 100 MPa over extended cycles,<sup>84,85</sup> demonstrating their suitability for high-pressure environments and long-term applications.

The evolution of net energy at constant pressures of 10 MPa and 100 MPa is analyzed for the  $\text{FASnI}_3$ -PVDF composite and various piezoelectric ceramics, as shown in Fig. 6. A discontinuous bar indicating the time required to complete a specific number of cycles at 20 Hz has also been added to provide a more tangible understanding of these values. It is important to note that these results assume that a piezoelectric material can endure the required number of cycles. However, given the uncertainty regarding the lifetime of the perovskite composite, it is crucial to explore the implications if the material cannot withstand such a high number of cycles, as discussed in the next section.

At 10 MPa, the halide perovskite composite requires less than 10<sup>6</sup> cycles to return the energy consumed during its fabrication, while the piezoelectric ceramics need cycles of 2–4 orders of magnitude more, see Fig. 6a. Among the PZT compositions, the PZT with a  $d_{33}$  coefficient similar to that of the perovskite offers the poorest performance in terms of recovering



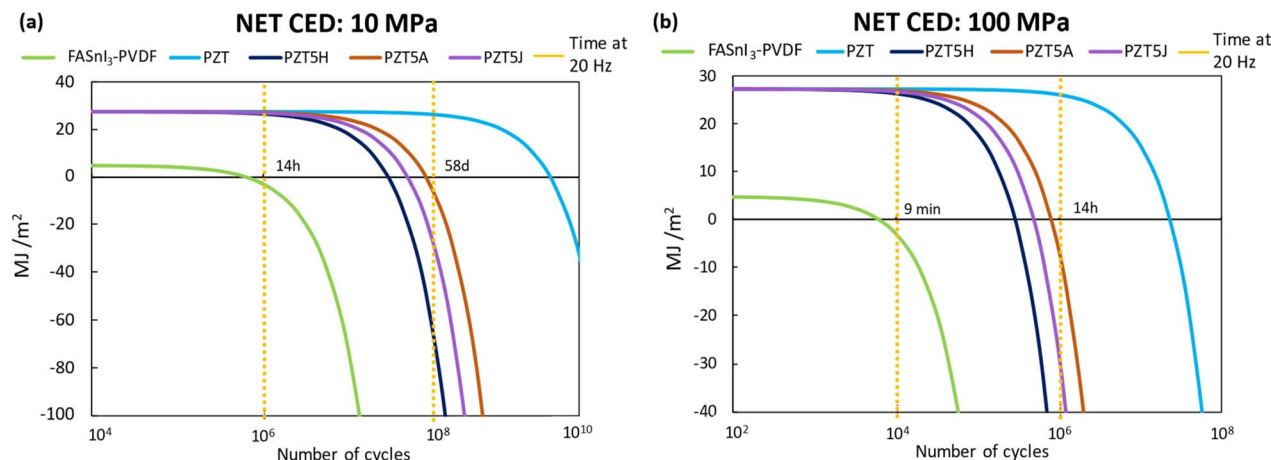


Fig. 6 NET cumulative energy demand of PZTs and FASnI<sub>3</sub>-PVDF perovskite, (a) at 10 MPa and (b) 100 MPa. The operating time is indicated next to the dashed line for a frequency of 20 Hz. Note that NET CED is calculated from eqn (6) and considering just the piezoelectric active layer.

the energy required for its fabrication. The commercial PZT ceramics exhibit a similar behavior, with PZT-5H showing the highest efficiency due to its high  $d_{33}$  coefficient, being able to return the energy consumed in its fabrication after  $10^7$  cycles, followed closely by PZT-5J and finally PZT-5A. At 100 MPa, the results are analogous, with the added benefit of recovering the energy investment much sooner due to the higher operating pressure, see Fig. 6b. The perovskite would need less than  $10^4$  cycles, while PZT-5H would require more than  $10^5$  cycles, and the PZT with a low  $d_{33}$  coefficient would require  $10^8$  cycles. Although the PZT-5H ceramics exhibit the highest room temperature piezoelectric properties and can reduce manufacturing impacts more quickly, this composition has a  $T_c$  value of 170 °C, which is very low compared to other materials. This can be a limiting factor for applications in systems where the device could be exposed to temperatures exceeding its Curie point.<sup>12,86</sup>

Fig. 6 shows that the FASnI<sub>3</sub>-PVDF composite material can recover the energy invested in its production significantly faster than piezoelectric ceramics under these conditions. This superior performance is attributed to its lower CED during fabrication, starting from a much smaller initial energy input. Additionally, the lower permeability of the perovskite enables it to generate more energy in open-circuit conditions.

We also analyze in Fig. S1† the time required for both materials to recover the energy consumed during their fabrication, considering only the energy harvested through energy harvesting and without accounting for the avoided impacts from replacing batteries. The recovery time is significantly longer under these conditions, being approximately two orders of magnitude higher compared to scenarios where the avoided impacts from battery replacement are included. The PZT-5H was selected to evaluate the remaining net impacts across various impact categories due to its superior operational performance. Comparisons were made with the FASnI<sub>3</sub>-PVDF composite and a PZT material exhibiting a  $d_{33}$  value similar to that of the perovskite-based composite. The calculations for these categories were carried out at a pressure of 10 MPa, as shown in Fig. 7. The categories of ecotoxicity and acidification

require fewer cycles to offset the impact produced during manufacturing, for both materials. In these categories, the halide perovskite needs approximately  $10^4$  cycles, while the PZT-5H requires more than  $10^6$  cycles. In terms of climate change and ecotoxicity, the duration needed to offset the environmental impact is longer. FASnI<sub>3</sub>-PVDF composite material requires  $10^5$  cycles to neutralize its impact, whereas the PZT-5H ceramic demands a substantially greater number of  $10^7$  cycles. While both materials are capable of mitigating their initial production impacts over time, the halide perovskite composite demonstrates significantly greater effectiveness in achieving substantial environmental benefits within a practical operational timeframe. This further underscores the superior potential of the halide perovskite composite in providing long-term sustainability compared to the PZT-5H ceramic. When comparing the PZT with a  $d_{33}$  value similar to that of the perovskite composite, its environmental performance is markedly worse across all categories. This material demands significantly more cycles to offset its initial production impacts.

Although piezoelectric materials as energy harvesters cannot generate as much energy as other renewable sources like solar power, they are indispensable in specific applications. For instance, replacing batteries in large-scale sensor networks can be costly and challenging, especially in hazardous or remote environments.<sup>87</sup> In this context, the FASnI<sub>3</sub>-PVDF composite not only exhibits lower initial environmental impacts but also enhances its environmental footprint by eliminating the need for batteries in specific applications in a shorter period of time. However, the longevity of perovskites still falls short of that of PZT ceramics. Literature reports that similar perovskite composites, such as MASnI<sub>3</sub>-PVDF, can endure up to  $10^4$  cycles under 0.5 MPa,<sup>88</sup> whereas PZT ceramics demonstrate significantly greater durability, with lifecycles ranging from  $10^7$  to  $10^{10}$  cycles in low-frequency applications.<sup>89–92</sup> This durability advantage of PZT ceramics highlights the importance of improving the operational lifespan of perovskite-based materials to fully realize their potential as sustainable alternatives in piezoelectric applications.



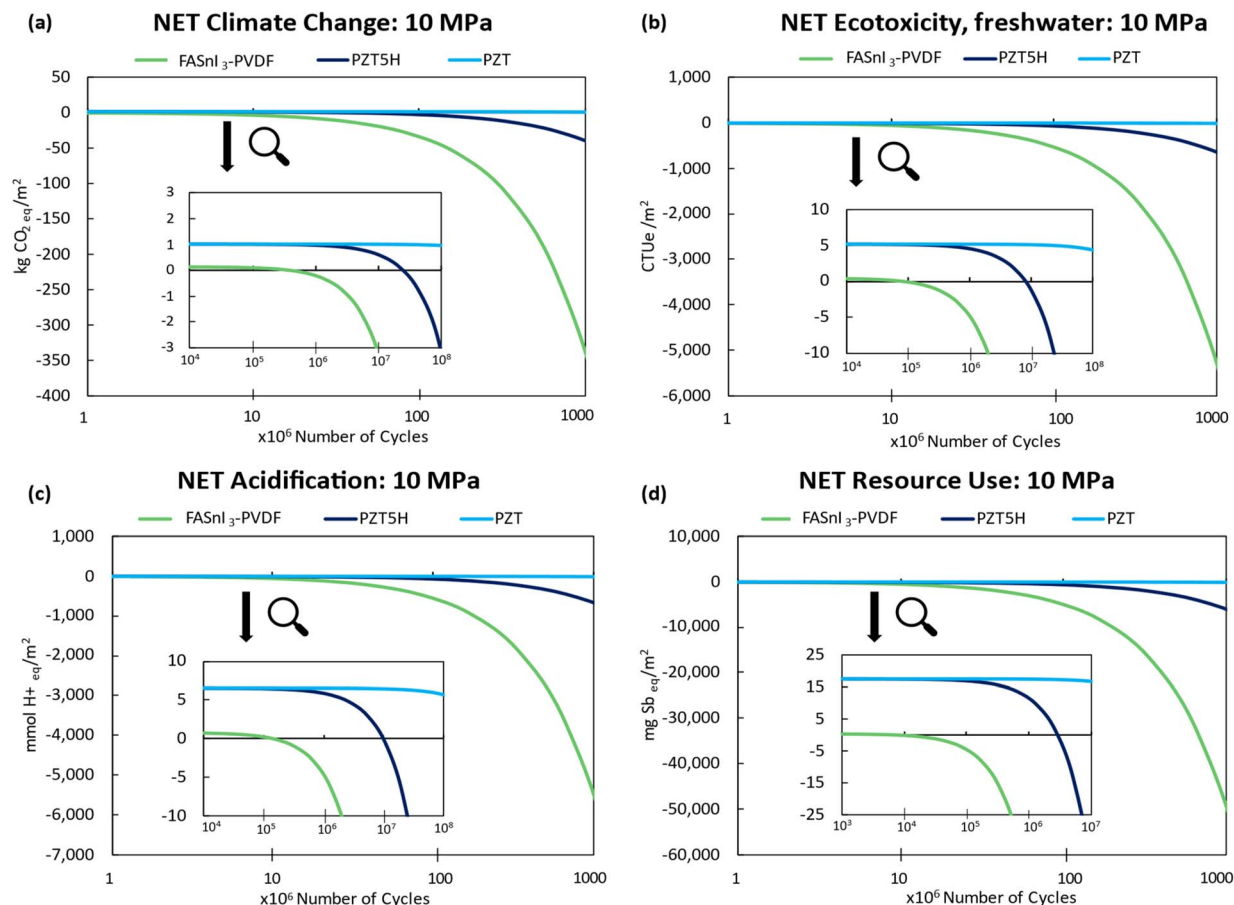


Fig. 7 Net environmental impacts of FASnI<sub>3</sub>-PVDF, PZT with similar  $d_{33}$  and PZT5H under a pressure of 10 MPa across multiple cycles: (a) climate change, (b) freshwater ecotoxicity, (c) acidification, and (d) resource use. Note that NET impacts are calculated from eqn (6) and considering just the piezoelectric active layer.

### 3.3. Environmental impacts from cradle-to-grave

Other impacts, which are not reflected in the conventional LCA, are the cases in which an accident occurs. The risk analysis allows us to assess the environmental impacts associated with such unforeseen events. Here we will assume that the device breaks and all the piezoelectric material is scattered on the ground.

In the scenario presented, the total environmental impact of the piezoelectric device is the combination of the impacts generated during its production (from cradle-to-gate) and those caused by its accidental release into the soil. The calculations show that 99.79% of the impact is in the human toxicity, non-cancer category for PZT result from its production, see Fig. 8a. While accidental release accounts for only 0.21% of the total impacts, it is noteworthy that lead is the dominant contributor, responsible for 99.99% of the non-cancer toxicity. This highlights the importance of considering the entire lifecycle and potential accidental releases when assessing the environmental impacts of piezoelectric materials.

Previous studies on piezoelectric materials have primarily concentrated on the environmental impacts associated with their manufacturing processes, often overlooking the impacts of their use and end-of-life stages. However, a cradle-to-grave analysis requires a comprehensive assessment that includes

end-of-life impacts, as this phase addresses disposal, recycling, and the potential release of hazardous substances. Fig. 8b and c presents a comparison of end-of-life impacts for both PZT ceramics and FASnI<sub>3</sub>-PVDF composite materials in the categories of climate change and CED. The results indicate that the perovskite-based composite generates roughly 34% of the impacts associated with the ceramic piezoelectrics. This difference primarily arises due to the end-of-life methods applied, which have a greater influence on the impact categories than the material composition itself. Furthermore, due to the lower density of halide perovskites, the perovskite composite demonstrates reduced environmental impacts per square meter, which is the functional unit adopted for this study. In terms of waste management, the recovery of PZT remains a major challenge. Although several recycling strategies have been proposed, they are still in early stages and face technical barriers such as energy-intensive processing and material contamination.<sup>93</sup> For example, a new recycling approach has been proposed where crushed PZT ceramics are reassembled using low-temperature sintering techniques, significantly reducing the energy demand compared to traditional processes. However, these methods are still proof-of-concept and unproven at industrial scale.<sup>94</sup> Moreover, the intrinsic lead



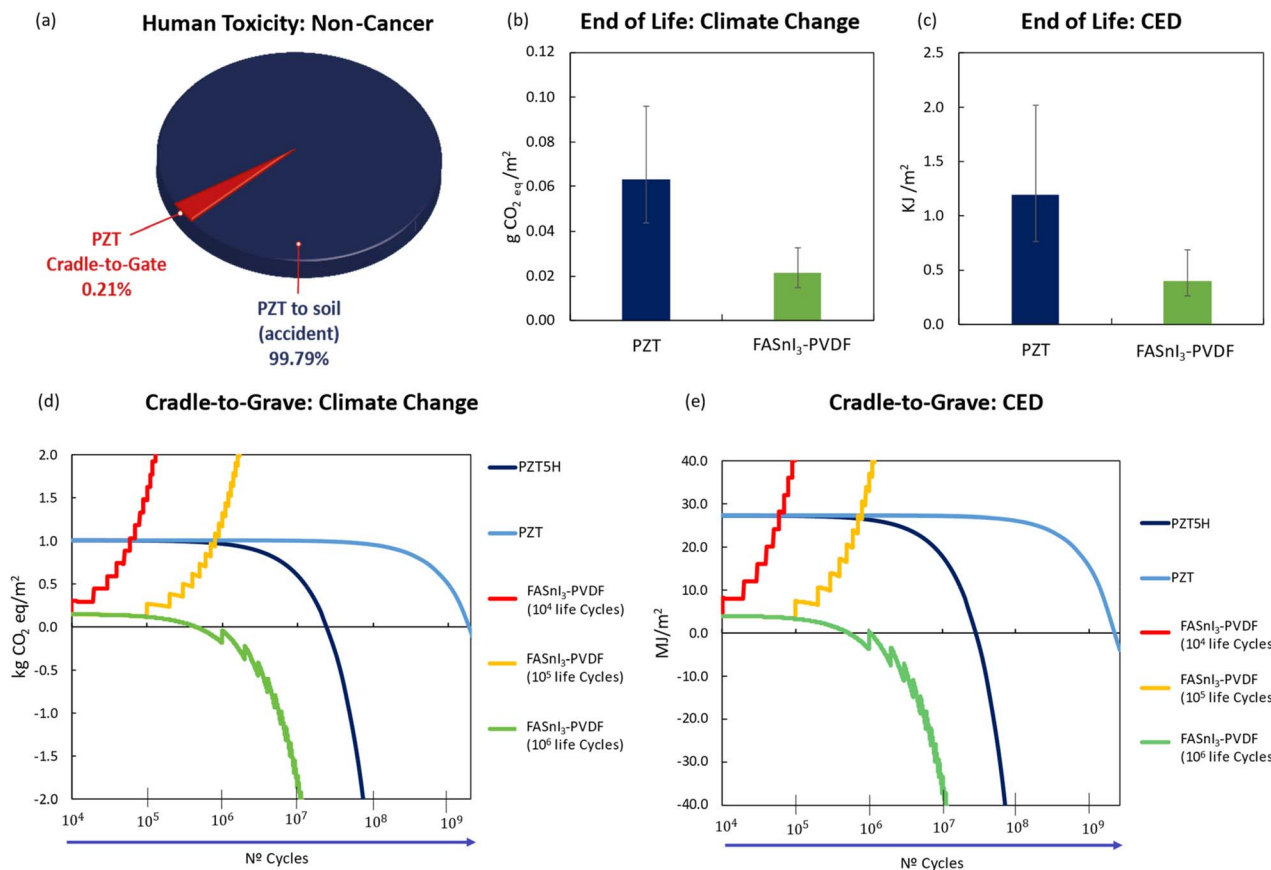


Fig. 8 (a) Comparison for Human toxicity: non-cancer impacts between cradle-to-gate impacts and accident soil releases; (b) end-of-life contribution to climate change for PZT and FASnI<sub>3</sub>-PVDF; (c) end-of-Life contribution to Cumulative Energy Demand (CED) for PZT and FASnI<sub>3</sub>-PVDF; (d) cradle-to-grave climate change impact as a function of the number of operational cycles; and (e) cradle-to-grave CED as a function of the number of operational cycles.

content of PZT poses serious environmental and regulatory challenges even if recycling were viable.

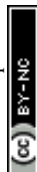
Recycling research is also emerging for halide perovskites. For example, a recent aqueous-based method demonstrated the separation of halogens from perovskite layers *via* distillation, enabling the recovery of valuable elements with minimal material degradation. Although these strategies are still just beginning, they illustrate the growing focus on enabling material circularity for lead-free perovskite technologies.<sup>95</sup> Similarly, PVDF recycling is already practiced in the context of silicon-based solar cells, where it is used as a backsheet. Several methods have been developed to recover PVDF from end-of-life photovoltaic modules, demonstrating its potential for separation and reuse.<sup>96</sup> However, many of these methods rely on pyrolysis, which, although effective in breaking down polymeric materials, requires high temperatures.<sup>97,98</sup> This leads to significant energy consumption and the release of harmful fluorine compounds, raising concerns about the environmental impact and safety of this recycling method.

In the cradle-to-grave analysis, a sensitivity study was conducted considering different lifetimes for the perovskite-based devices, see Fig. 8d and e, assuming operation at 10 MPa. The scenarios evaluated include a currently reported lead-free perovskite lifetime of 10<sup>4</sup> cycles,<sup>88</sup> as well as extended

lifetimes of 10<sup>5</sup> and 10<sup>6</sup> cycles. At the end of the device's operational life, replacing the FASnI<sub>3</sub>-PVDF piezoelectric with additional units is required to meet the desired number of cycles. In these scenarios, eqn (6) and (7) are also applied to calculate the avoided impacts associated with not using conventional batteries.

For 10<sup>4</sup> cycles, all scenarios involving the FASnI<sub>3</sub>-PVDF composite exhibit a lower environmental impact compared to PZT. However, for 10<sup>5</sup> cycles, the composite with a lifetime of 10<sup>4</sup> cycles matches the impact of PZT due to the need for 10 additional devices to achieve the required operational duration. Similarly, for 10<sup>6</sup> cycles, the composite with a lifetime of 10<sup>5</sup> cycles reaches the same environmental impact as PZT.

As a result, for lifetimes of 10<sup>4</sup> and 10<sup>5</sup> cycles, the halide perovskite system struggles to mitigate the environmental impacts associated with manufacturing multiple devices to meet the required cycles. In these scenarios, both PZT5H and the PZT material with a  $d_{33}$  similar to that of the FASnI<sub>3</sub>-PVDF composite demonstrate better environmental performance. However, for a lifetime of 10<sup>6</sup> cycles, the halide perovskite composite achieves a sufficiently long operational period to offset its production impacts, making it a competitive alternative. In contrast, PZT5H would require over 10<sup>7</sup> cycles, and the PZT with similar  $d_{33}$  would





need an even higher number of cycles to achieve a comparable level of environmental impact mitigation.

### 3.4. Toxicity issues

The main toxicity problem of PZT is lead, this material is toxic to reproduction and is listed as a substance of very high concern (SVHC) by the European Chemical Agency (ECHA) under the REACH regulation and there are also reports indicating that lead is likely carcinogenic to humans.<sup>99</sup>

Moreover, the fabrication of these piezoelectric ceramics requires high temperatures, which introduces further risks and significantly increases energy consumption. In contrast, Pb-free halide perovskite materials can be produced at ambient temperatures, significantly reducing associated hazards and energy demands. There is a study that has examined the human toxicity and ecotoxicity of perovskite solar cells (PSCs), and the results indicate that PbI and PbO exhibit very similar toxicity levels in these aspects. Therefore, producing Pb-based halide perovskites might not be a favorable option, and it would be better to avoid the use of lead altogether.<sup>100</sup> Additionally, when evaluating alternatives to replace Pb in PCSs, Sn emerges as a less toxic option due to its degradation into the environmentally benign compound SnO<sub>2</sub> upon exposure to air.<sup>101,102</sup>

The main challenge in fully adopting the substitution of lead with tin-based materials lies in establishing characterization factors for human health impact categories related to tin, which are currently unavailable. Critical effects such as neurotoxicity and carcinogenicity remain under debate, creating a significant gap in assessing the environmental and health impacts of tin-based perovskites. Without these toxicity factors, it is not possible to make a fair comparison between lead-based and tin-based materials in terms of human toxicity.

Meanwhile, halide perovskite-based materials show promise due to their lower environmental impact compared to traditional PZT ceramics, it is also important to consider the toxicity of the solvents used in their production. The most commonly used solvent for perovskite layer deposition, *N,N*-dimethylformamide (DMF), is listed as a substance of very high concern (SVHC) by the European Chemical Agency under the REACH regulation.<sup>103</sup> For FASnI<sub>3</sub> perovskite, DMF contributes approximately 20% of the environmental impacts associated with perovskite fabrication, emphasizing the importance of exploring alternative solvents to mitigate these impacts. Studies suggest that dimethyl sulfoxide (DMSO), a less toxic solvent, could serve as a suitable alternative.<sup>104</sup> Formulations incorporating this solvent, such as a DMSO : DMF (9 : 1, v/v) mixture,<sup>105</sup> have been developed to significantly reduce DMF usage, thereby further minimizing the environmental footprint of halide perovskite production. This highlights the importance of replacing SVHCs with less dangerous substances or technologies wherever feasible. Consequently, there is a critical need for further research and development in identifying and utilizing safer alternatives in the production of halide perovskite materials to minimize their overall environmental and health impacts. In particular, PVDF is chemically related to per- and polyfluoroalkyl substances (PFAS), a group of persistent and

bioaccumulative compounds increasingly scrutinized due to their toxicity and resistance to degradation. While PVDF is not currently classified as hazardous under the ECHA's harmonized classification system. No hazards have been officially recognized but some health risks are routinely reported including skin and eye irritation and respiratory effects.<sup>106</sup> As part of its broader PFAS restriction strategy, ECHA is expected to assess possible regulatory measures specifically targeting PVDF by the end of 2025<sup>107</sup> This anticipated regulatory development underscores the importance of monitoring policy changes and exploring non-fluorinated alternatives for future applications.

### 3.5. Limitation of the study

This study acknowledges some limitations that should be considered when interpreting the results. The data used for the LCA was primarily derived from existing literature, and future work should aim to collect more primary data specific to the systems under study. The calculations involve assumptions that could impact the accuracy of the results, such as energy consumption, which may not reflect the specific conditions of all manufacturing environments. One important and critical limitation pertains to the durability of halide perovskite materials, which may not withstand as many cycles, temperatures, and pressures as traditional piezoelectric ceramics like PZT. This is particularly important in high-pressure and long-life applications, as halides perovskites might not sustain, at the current state of development, their performance long enough to offset the energy required for their production. Further research into enhancing the durability of halide perovskites is necessary to address this issue. Here Sn based halide perovskite piezoelectric devices can take advantage of the enormous progress on reported stability for Sn-based perovskite solar cells,<sup>105,108</sup> and increase in the lifetime cycles in near future can be anticipated.

Additionally, the end-of-life treatment of both PZT and halide perovskite materials includes considerations for disposal in safety landfills, introducing variability based on local regulations, landfill technologies, and material composition. This aspect introduces additional uncertainty into the LCA and highlights the need for improved recycling and disposal strategies to mitigate potential environmental harm. Other components that encompass the final product, such as electrodes or substrates, have not been considered. There are numerous possibilities for these layers, and it would be valuable to study their impact on environmental effects in the future.

These limitations underscore the necessity for ongoing research and development to refine life cycle assessments of piezoelectric materials, particularly in the context of emerging lead-free alternatives like tin-based halide perovskites. Addressing these challenges will be crucial for accurately evaluating their environmental performance and potential for sustainable applications.

## 4. Conclusions

In the realm of piezoelectric materials, it is essential, and even mandatory under European regulations, to pursue lead-free



solutions. This study specifically aimed to assess whether FASnI<sub>3</sub>-PVDF halide perovskite composites could serve as a more sustainable alternative to conventional lead-based PZT ceramics.

A detailed examination of the manufacturing processes reveals that the raw materials used in PZT production generate significantly higher environmental impacts than those required for lead-free halide perovskites, driven in part by the inclusion of lead, especially in the categories related to toxicity. Additionally, PZT ceramic production involves high-temperature processes, resulting in greater energy consumption and elevated manufacturing risks. In contrast, the synthesis of halide perovskites occurs at much lower temperatures (approximately 100 °C), making it a safer and less energy-intensive process. Notably, the fabrication of FASnI<sub>3</sub>-PVDF composites generates less than 20% of the environmental impacts associated with conventional PZT ceramics, or even less for certain impacts.

For thin-film devices, halide perovskites composites also support more energy-efficient deposition techniques which not only reduce energy costs for manufacturers but also significantly lower the overall environmental footprint. These advancements align with the overarching goal of developing sustainable, lead-free piezoelectric materials.

The application of these devices in energy harvesting further highlights their benefits. By using these materials, the continuous replacement of batteries in complex environments where consistent energy supply is necessary, such as sensor systems, can be avoided. Halide perovskites or their composites, in particular, offer significant advantages due to their low energy requirements for fabrication and reduced permeability. The FASnI<sub>3</sub>-PVDF composite achieves a competitive environmental advantage over conventional batteries when it operates for a lifetime of at least 10<sup>6</sup> cycles for 10 MPa (tire pressure), as this duration offsets the environmental impacts of its manufacturing, least 10<sup>4</sup> cycles for 100 MPa.

Our findings demonstrate that FASnI<sub>3</sub>-PVDF composites have significant potential for sustainable piezoelectric energy harvesting. This highlights lead-free halide perovskites as promising solutions for energy harvesting applications and represents a step toward more environmentally responsible technologies.

## Data availability

All data relevant to this article are available within the main text and the ESI† and in our Zenodo repository at <https://doi.org/10.5281/zenodo.14756480>.

## Conflicts of interest

There are no conflicts to declare.

## Acknowledgements

The authors acknowledge financial support from Generalitat Valenciana (Prometeo Grant Q-SOLUTIONS, ref CIPROM/2021/

078), Next Generation EU Advanced Materials Grant (PRINT-P, ref MFA/2022/020) and European Research Council (ERC) under the European Union's Horizon 2020 Research and Innovation Program (CREATE, Grant Agreement No. 852722).

## References

- 1 J. Curie and P. Curie, *Bull. Soc. Fr. Minéral.*, 1880, **3**, 90–93, DOI: [10.3406/bulmi.1880.1564](#).
- 2 J. Chen, S. K. Oh, H. Zou, S. Shervin, W. Wang, S. Pouladi, Y. Zi, Z. L. Wang and J. H. Ryou, *ACS Appl. Mater. Interfaces*, 2018, **10**, 12839–12846, DOI: [10.1021/acsnano.1c06849](#).
- 3 J. F. Tressler, S. Alkoy and R. E. Newnham, *J. Electroceram.*, 1998, **2**, 257–272, DOI: [10.1023/A:1009926623551](#).
- 4 L. P. Wang, R. A. Wolf, Y. Wang, K. K. Deng, L. Zou, R. J. Davis and S. Trolier-McKinstry, *J. Microelectromech. Syst.*, 2003, **12**, 433–439, DOI: [10.1109/jmems.2003.811749](#).
- 5 B. L. Turner, S. Senevirathne, K. Kilgour, D. McArt, M. Biggs, S. Menegatti and M. A. Daniele, *Adv. Healthcare Mater.*, 2021, **10**, 2100986, DOI: [10.1002/adhm.202100986](#).
- 6 X. Gao, J. Yang, J. Wu, X. Xin, Z. Li, X. Yuan, X. Shen, S. Dong, X. Gao, J. Yang, J. Wu, X. Xin, Z. Li, X. Yuan, X. Shen and S. Dong, *Adv. Mater. Technol.*, 2020, **5**, 1900716, DOI: [10.1002/admt.201900716](#).
- 7 V. N. Bindal and M. F. Chandra, *J. Opt.*, 1976, **5**(3), 51–55, DOI: [10.1007/BF03548967](#).
- 8 J. Wang, X. Qin, Z. Liu, K. Shi, G. Ding, X. Li and G. Cai, *Smart Mater. Struct.*, 2022, **31**, 055003, DOI: [10.1088/1361-665X/AC51AD](#).
- 9 M. Gholikhani, H. Roshani, S. Dessouky and A. T. Papagiannakis, *Appl. Energy*, 2020, **261**, 114388, DOI: [10.1016/j.apenergy.2019.114388](#).
- 10 Y. Liu, H. Khanbarez, M. A. Halim, A. Feeney, X. Zhang, H. Heidari and R. Ghannam, *Nano Sel.*, 2021, **2**, 1459–1479, DOI: [10.1002/nano.202000242](#).
- 11 Piezoelectric devices market size global report, 2022 - 2030, <https://www.polarismarketresearch.com/industry-analysis/piezoelectric-devices-market>, accessed 23 July 2024.
- 12 M. W. Hooker, *Properties of PZT-Based Piezoelectric Ceramics Between-150 and 250 °C*, 1998.
- 13 Y. Yu, X. Wang and X. Yao, *Ferroelectrics*, 2013, **451**, 96–102, DOI: [10.1080/00150193.2013.839249](#).
- 14 H. Jaffe, *J. Am. Ceram. Soc.*, 1958, **41**, 494–498, DOI: [10.1111/J.1151-2916.1958.TB12903.X](#).
- 15 S. S. Chandratreya, R. M. Fulrath and J. A. Pask, *J. Am. Ceram. Soc.*, 1981, **64**, 422–425, DOI: [10.1111/J.1151-2916.1981.TB09883.X](#).
- 16 M. D. Nguyen, E. P. Houwman, M. Dekkers and G. Rijnders, *ACS Appl. Mater. Interfaces*, 2017, **9**, 9849–9861, DOI: [10.1021/acsnano.1c06849](#).
- 17 M. D. Nguyen, M. Dekkers, H. N. Vu and G. Rijnders, *Sens. Actuators, A*, 2013, **199**, 98–105, DOI: [10.1016/J.SNA.2013.05.004](#).
- 18 K. Tsuchiya, T. Kitagawa and E. Nakamachi, *Precis. Eng.*, 2003, **27**, 258–264, DOI: [10.1016/S0141-6359\(03\)00006-0](#).
- 19 European Commission, Restriction of Hazardous Substances in Electrical and Electronic Equipment



- (RoHS), [https://environment.ec.europa.eu/topics/waste-and-recycling/rohs-directive\\_en](https://environment.ec.europa.eu/topics/waste-and-recycling/rohs-directive_en), accessed 11 June 2024.
- 20 European Commission, Waste from electrical and electronic equipment (WEEE), [https://environment.ec.europa.eu/topics/waste-and-recycling/waste-electrical-and-electronic-equipment-weee\\_en](https://environment.ec.europa.eu/topics/waste-and-recycling/waste-electrical-and-electronic-equipment-weee_en), accessed 11 June 2024.
  - 21 European Commission, Implementation of the RoHS Directive, [https://environment.ec.europa.eu/topics/waste-and-recycling/rohs-directive/implementation-rohs-directive\\_en](https://environment.ec.europa.eu/topics/waste-and-recycling/rohs-directive/implementation-rohs-directive_en), accessed 25 April 2025.
  - 22 EU: RoHS exemptions update, <https://www.globalnorm.de/en/news-product-compliance/details/eu-rohs-exemptions-update-1-2025/>, accessed 25 April 2025.
  - 23 S. Ippili, V. Jella, A. M. Thomas and S.-G. Yoon, *Nanoenergy Adv.*, 2021, **1**, 3–31, DOI: [10.3390/nanoenergyadv1010002](https://doi.org/10.3390/nanoenergyadv1010002).
  - 24 V. Jella, S. Ippili, J. H. Eom, J. Choi and S. G. Yoon, *Nano Energy*, 2018, **53**, 46–56, DOI: [10.1016/j.nanoen.2018.08.033](https://doi.org/10.1016/j.nanoen.2018.08.033).
  - 25 H. Park, C. Ha and J.-H. Lee, *J. Mater. Chem. A*, 2020, **8**, 24353–24367, DOI: [10.1039/d0ta08780g](https://doi.org/10.1039/d0ta08780g).
  - 26 E. Reyes-Francis, C. Echeverría-Arrondo, D. Esparza, T. López-Luke, T. Soto-Montero, M. Morales-Masis, S. H. Turren-Cruz, I. Mora-Seró and B. Julián-López, *Chem. Mater.*, 2024, **36**, 1728–1736, DOI: [10.1021/acs.chemmater.3c03108](https://doi.org/10.1021/acs.chemmater.3c03108).
  - 27 V. Jella, S. Ippili, J. H. Eom, S. V. N. Pammi, J. S. Jung, V. D. Tran, V. H. Nguyen, A. Kirakosyan, S. Yun, D. Kim, M. R. Sihn, J. Choi, Y. J. Kim, H. J. Kim and S. G. Yoon, *Nano Energy*, 2019, **57**, 74–93, DOI: [10.1016/j.nanoen.2018.12.038](https://doi.org/10.1016/j.nanoen.2018.12.038).
  - 28 Y.-M. You, W.-Q. Liao, D. Zhao, H.-Y. Ye, Y. Zhang, Q. Zhou, X. Niu, J. Wang, P.-F. Li, D.-W. Fu, Z. Wang, S. Gao, K. Yang, J.-M. Liu, J. Li, Y. Yan and R.-G. Xiong, *Science*, 2017, **357**, 306–309, DOI: [10.1126/science.aai8535](https://doi.org/10.1126/science.aai8535).
  - 29 G. Huang, A. A. Khan, M. M. Rana, C. Xu, S. Xu, R. Saritas, S. Zhang, E. Abdel-Rahmand, P. Turban, S. Ababou-Girard, C. Wang and D. Ban, *ACS Energy Lett.*, 2021, **6**, 16–23, DOI: [10.1021/acsenenergylett.0c02200](https://doi.org/10.1021/acsenenergylett.0c02200).
  - 30 E. K. Akdogan, M. Allahverdi and A. Safari, *IEEE Trans. Ultrason. Ferroelectr. Freq. Control*, 2005, **52**, 746–775, DOI: [10.1109/TUFFC.2005.1503962](https://doi.org/10.1109/TUFFC.2005.1503962).
  - 31 K. Shi, B. Chai, H. Zou, P. Shen, B. Sun, P. Jiang, Z. Shi and X. Huang, *Nano Energy*, 2021, **80**, 105515, DOI: [10.1016/j.nanoen.2020.105515](https://doi.org/10.1016/j.nanoen.2020.105515).
  - 32 B. Dai, G. M. Biesold, M. Zhang, H. Zou, Y. Ding, Z. L. Wang and Z. Lin, *Chem. Soc. Rev.*, 2021, **50**, 13646–13691, DOI: [10.1039/D1CS00506E](https://doi.org/10.1039/D1CS00506E).
  - 33 J. Inderherbergh, *Ferroelectrics*, 1991, **115**, 295–302, DOI: [10.1080/00150193.1991.11876614](https://doi.org/10.1080/00150193.1991.11876614).
  - 34 R. Pandey, G. SB, S. Grover, S. K. Singh, A. Kadam, S. Ogale, U. V. Waghmare, V. R. Rao and D. Kabra, *ACS Energy Lett.*, 2019, **4**, 1004–1011, DOI: [10.1021/acsenenergylett.9b00323](https://doi.org/10.1021/acsenenergylett.9b00323).
  - 35 H. Kobayashi, K. Matsuoka, T. Tsuyuki, A. Suzuki, I. Kimura, T. Jinbo and K. Suu, *Proceedings of the IEEE International Conference on Micro Electro Mechanical Systems (MEMS)*, 2020, pp. 550–553, DOI: [10.1109/MEMS46641.2020.9056215](https://doi.org/10.1109/MEMS46641.2020.9056215).
  - 36 N.-I. Kim, J. M. Lee, M. Moradnia, J. Chen, S. Pouladi, M. Yarali, J. Y. Kim, M.-K. Kwon, T. R. Lee and J.-H. Ryou, *Soft Sci.*, 2022, **2**, 8, DOI: [10.20517/ss.2022.06](https://doi.org/10.20517/ss.2022.06).
  - 37 G. T. Hwang, M. Byun, C. K. Jeong and K. J. Lee, *Adv. Healthcare Mater.*, 2015, **4**, 646–658, DOI: [10.1002/ADHM.201400642](https://doi.org/10.1002/ADHM.201400642).
  - 38 T. Ibn-Mohammed, S. C. L. Koh, I. M. Reaney, A. Acquaye, D. Wang, S. Taylor and A. Genovese, *Energy Environ. Sci.*, 2016, **9**, 3495–3520, DOI: [10.1039/C6EE02429G](https://doi.org/10.1039/C6EE02429G).
  - 39 T. Ibn-Mohammed, I. M. Reaney, S. C. L. Koh, A. Acquaye, D. C. Sinclair, C. A. Randall, F. H. Abubakar, L. Smith, G. Schileo and L. Ozawa-Meida, *J. Eur. Ceram. Soc.*, 2018, **38**, 4922–4938, DOI: [10.1016/j.jeurceramsoc.2018.06.044](https://doi.org/10.1016/j.jeurceramsoc.2018.06.044).
  - 40 L. Smith, T. Ibn-Mohammed, L. Koh and I. M. Reaney, *J. Am. Ceram. Soc.*, 2019, **102**, 7037–7064, DOI: [10.1111/JACE.16712](https://doi.org/10.1111/JACE.16712).
  - 41 S. Hazeri, PhD thesis, Concordia University, 2017.
  - 42 S. Hazeri and C. N. Mulligan, *AIP Adv.*, 2022, **12**, 65112, DOI: [10.1063/5.0086778](https://doi.org/10.1063/5.0086778).
  - 43 Y. Wu, P. S. Soon, J. T. Lu, J. Zhou, Y. X. Liu, Z. Guo, K. Wang and W. Gong, *EcoMat*, 2024, **6**(5), e12450, DOI: [10.1002/eom2.12450](https://doi.org/10.1002/eom2.12450).
  - 44 R. Sekhar Muddam, J. Sinclair and L. Krishnan Jagadamma, *Materials*, 2024, **17**, 3083, DOI: [10.3390/ma17133083](https://doi.org/10.3390/ma17133083).
  - 45 ISO 14040:2006, *Environmental Management — Life Cycle Assessment — Principles and Framework*.
  - 46 ISO 14044:2006, *Environmental Management — Life Cycle Assessment — Requirements and Guidelines*.
  - 47 T. Ibn-Mohammed, F. A. Yamoah, A. Acquaye, K. Omoteso and S. C. L. Koh, *Resour., Conserv. Recycl.*, 2024, **205**, 107523, DOI: [10.1016/j.resconrec.2024.107523](https://doi.org/10.1016/j.resconrec.2024.107523).
  - 48 Doka LCA | Home, <https://www.doka.ch/home.htm>, accessed 19 April 2024.
  - 49 M. A. Parvez Mahmud, N. Huda, S. Hisan Farjana and C. Lang, in *IOP Conference Series: Earth and Environmental Science*, IOP Publishing, 2018, vol. 154, p. 012017, DOI: [10.1088/1755-1315/154/1/012017](https://doi.org/10.1088/1755-1315/154/1/012017).
  - 50 A. L. Kholkin, I. K. Bdikin, D. A. Kiselev, V. V. Shvartsman and S.-H. Kim, *J. Electroceram.*, 2007, **19**, 83–96, DOI: [10.1007/s10832-007-9045-2](https://doi.org/10.1007/s10832-007-9045-2).
  - 51 X. Yan, M. Zheng, M. Zhu and Y. Hou, *Crystals*, 2020, **10**, 1–9, DOI: [10.3390/cryst10100907](https://doi.org/10.3390/cryst10100907).
  - 52 S. Shahab, S. Zhao and A. Erturk, *Energy Technol.*, 2018, **6**, 935–942, DOI: [10.1002/ente.201700873](https://doi.org/10.1002/ente.201700873).
  - 53 Piezo Support, Material Properties, <https://support.piezo.com/article/62-material-properties>, accessed 10 April 2024.
  - 54 Ecoinvent Centre, Ecoinvent Database v3.9, <https://support.ecoinvent.org/ecoinvent-version-3.9>, accessed 12 December 2024.
  - 55 Y. Wu and T. Feng, *J. Alloys Compd.*, 2010, **491**, 452–455, DOI: [10.1016/j.jallcom.2009.10.222](https://doi.org/10.1016/j.jallcom.2009.10.222).
  - 56 E. F. Mantheakis, B. H. Watson Iii, M. J. Brova, G. L. Messing, L. A. Stoica and I. M. Reaney, *J. Mater. Sci.*, 2023, **58**, 5693–5704, DOI: [10.1007/s10853-023-08335-4](https://doi.org/10.1007/s10853-023-08335-4).





- 57 F. Piccinno, R. Hischier, S. Seeger and C. Som, *J. Cleaner Prod.*, 2016, **135**, 1085–1097, DOI: [10.1016/j.jclepro.2016.06.164](#).
- 58 T. Rödiger, A. Schönecker and G. Gerlach, *J. Am. Ceram. Soc.*, 2010, **93**, 901–912, DOI: [10.1111/j.1551-2916.2010.03702.x](#).
- 59 A. Kotliarenko, O. Azzolini, G. Keppel, C. Pira and J. Esposito, *Appl. Sci.*, 2021, **11**, 9219, DOI: [10.3390/AP11199219](#).
- 60 P. Čulík, K. Brooks, C. Momblona, M. Adams, S. Kinge, F. Maréchal, P. J. Dyson and M. K. Nazeeruddin, *ACS Energy Lett.*, 2022, **7**, 3039–3044, DOI: [10.1021/acsenenergylett.2c01728](#).
- 61 N. Wu, Q. Wang and S. T. Quek, *J. Sound Vib.*, 2010, **329**, 1126–1136, DOI: [10.1016/j.jsv.2009.10.040](#).
- 62 D. G. Wakshume and M. Ł. Placzek, *Electronics*, 2024, **13**(5), DOI: [10.3390/electronics13050987](#).
- 63 J. Chen, Y. Dai, S. Kang, L. Xu and S. Gao, *IEEE Sens. J.*, 2021, **21**, 26364–26372, DOI: [10.1109/JSEN.2021.3064235](#).
- 64 T. Li and P. S. Lee, *Small Struct.*, 2022, **3**, 2100128, DOI: [10.1002/SSTR.202100128](#).
- 65 V. Jella, S. Ippili and S. G. Yoon, *ACS Appl. Electron. Mater.*, 2020, **2**, 2579–2590, DOI: [10.1021/acsaelm.0C00473](#).
- 66 G. A. Lesieutre, G. K. Ottman and H. F. Hofmann, *J. Sound Vib.*, 2004, **269**, 991–1001, DOI: [10.1016/S0022-460X\(03\)00210-4](#).
- 67 Z. Li, J. Roscow, H. Khanbareh, J. Taylor, G. Haswell and C. Bowen, *Mater. Today Energy*, 2023, **37**, 101396, DOI: [10.1016/j.mtener.2023.101396](#).
- 68 R. G. Sabat, B. K. Mukherjee, W. Ren and G. Yang, *J. Appl. Phys.*, 2007, **101**(6), DOI: [10.1063/1.2560441](#).
- 69 A. Morel, G. Pillonnet, Y. Wanderoild and A. Badel, *J. Low Power Electron.*, 2018, **14**, 244–254, DOI: [10.1166/jolpe.2018.1562](#).
- 70 J. I. Roscow, H. Pearce, H. Khanbareh, S. Kar-Narayan and C. R. Bowen, *Eur. Phys. J.: Spec. Top.*, 2019, **228**(7), 1537–1554, DOI: [10.1140/EPJST/E2019-800143-7](#).
- 71 R. A. Wolf and S. Trolier-McKinstry, *J. Appl. Phys.*, 2004, **95**, 1397–1406, DOI: [10.1063/1.1636530](#).
- 72 R. Frischknecht, N. Jungbluth, H.-J. Althaus, G. Doka, R. Dones, T. Heck, S. Hellweg, R. Hischier, T. Nemecek, G. Rebitzer, M. Spielmann and G. Wernet, *Overview and Methodology. Data v2.0 (2007). Ecoinvent Report No. 1*, 2007.
- 73 Y. Deng, L. Liu, Y. Cheng, C. W. Nan and S. J. Zhao, *Mater. Lett.*, 2003, **57**, 1675–1678, DOI: [10.1016/S0167-577X\(02\)01050-9](#).
- 74 K. Rama Mohana Rao, A. V. Prasada Rao and S. Komarneni, *Mater. Lett.*, 1996, **28**, 463–467, DOI: [10.1016/0167-577X\(96\)00106-1](#).
- 75 Y. Kinemuchi, T. Ikeuchi, T. Suzuki, H. Suematsu, W. Jiang and K. Yatsui, *IEEE Trans. Plasma Sci.*, 2002, **30**, 1858–1862, DOI: [10.1109/TPS.2002.805374](#).
- 76 I. Bakaimi, B. E. Hayden, C. J. Mitchell and G. Z. Mashanovich, *Thin Solid Films*, 2024, **791**, 140239, DOI: [10.1016/j.tsf.2024.140239](#).
- 77 F. Rubio-Marcos, R. López-Juárez, R. E. Rojas-Hernandez, A. Del Campo, N. Razo-Pérez and J. F. Fernandez, *ACS Appl. Mater. Interfaces*, 2015, **7**, 23080–23088, DOI: [10.1021/acsami.5b06747](#).
- 78 Z. Li, X. Peng, G. Hu, D. Zhang, Z. Xu, Y. Peng and S. Xie, *Energy Convers. Manag.*, 2022, **258**, 115466, DOI: [10.1016/j.enconman.2022.115466](#).
- 79 H. Yuan, S. Wang, C. Wang, Z. Song and Y. Li, *Appl. Energy*, 2022, **306**, 118153, DOI: [10.1016/j.apenergy.2021.118153](#).
- 80 F. Yildiz and K. Baltaci, in *ASEE Annual Conference & Exposition*, 2015, pp. 265991–2659914.
- 81 S. K. Ghosh and D. Mandal, *Nano Energy*, 2016, **28**, 356–365, DOI: [10.1016/j.nanoen.2016.08.030](#).
- 82 A. Jasim, G. Yesner, H. Wang, A. Safari, A. Maher and B. Basily, *Appl. Energy*, 2018, **224**, 438–447, DOI: [10.1016/j.apenergy.2018.05.040](#).
- 83 J. Wang, F. Xiao and H. Zhao, *Renew. Sustain. Energy Rev.*, 2021, **151**, 111522, DOI: [10.1016/j.rser.2021.111522](#).
- 84 N. Aruchamy, T. Schenk, V. Kovacova, S. Glinsek, E. Defay and T. Granzow, *J. Eur. Ceram. Soc.*, 2021, **41**, 6991–6999, DOI: [10.1016/j.jeurceramsoc.2021.07.010](#).
- 85 S. Mall and J. M. Coleman, *Smart Mater. Struct.*, 1998, **7**, 822, DOI: [10.1088/0964-1726/7/6/010](#).
- 86 D. V. Kuzenko, *J. Adv. Dielectr.*, 2021, **11**, DOI: [10.1142/S2010135X21500065](#).
- 87 S. Priya, H. C. Song, Y. Zhou, R. Varghese, A. Chopra, S. G. Kim, I. Kanno, L. Wu, D. S. Ha, J. Ryu and R. G. Polcawich, *Energy Harvest. Syst.*, 2019, **4**, 3–39, DOI: [10.1515/ehs-2016-0028](#).
- 88 S. Ippili, V. Jella, J. H. Eom, J. Kim, S. Hong, J. S. Choi, V. D. Tran, N. Van Hieu, Y. J. Kim, H. J. Kim and S. G. Yoon, *Nano Energy*, 2019, **57**, 911–923, DOI: [10.1016/j.nanoen.2019.01.005](#).
- 89 A. Mazzalai, D. Balma, N. Chidambaram, R. Matloub and P. Muralt, *J. Microelectromech. Syst.*, 2015, **24**, 831–838, DOI: [10.1109/JMEMS.2014.2353855](#).
- 90 R. Salazar, M. Serrano and A. Abdelkefi, *Appl. Energy*, 2020, **270**, 115161, DOI: [10.1016/j.apenergy.2020.115161](#).
- 91 R. Salazar, K. Larkin and A. Abdelkefi, *Mech. Syst. Signal Process.*, 2021, **156**, 107697, DOI: [10.1016/j.ymssp.2021.107697](#).
- 92 M. D. Nguyen, E. P. Houwman and G. Rijnders, *Sci. Rep.*, 2017, **7**(1), 1–9, DOI: [10.1038/s41598-017-13425-w](#).
- 93 S. S. Anandakrishnan, S. Yadav, M. Tabeshfar, V. Balanov, T. Kaushalya, M. Nelo, J. Peräntie, J. Juuti and Y. Bai, *Glob. Chall.*, 2023, **7**, 2300061, DOI: [10.1002/GCH2.202300061](#).
- 94 S. S. Anandakrishnan, M. Tabeshfar, M. Nelo, J. Peräntie, H. Jantunen, J. Juuti and Y. Bai, *RSC Sustainability*, 2024, **2**, 961–974, DOI: [10.1039/D3SU00348E](#).
- 95 X. Xiao, N. Xu, X. Tian, T. Zhang, B. Wang, X. Wang, Y. Xian, C. Lu, X. Ou, Y. Yan, L. Sun, F. You and F. Gao, *Nature*, 2025, **638**(8051), 670–675, DOI: [10.1038/s41586-024-08408-7](#).
- 96 P. Su, Y. He, Y. Feng, Q. Wan and T. Li, *Sol. Energy Mater. Sol. Cells*, 2024, **277**, 113109, DOI: [10.1016/J.SOLMAT.2024.113109](#).
- 97 K. K. Patel and S. Mallick, *Circ. Econ. Sustainability*, 2024, **4**, 1835–1850, DOI: [10.1007/S43615-024-00361-X/FIGURES/10](#).





- 98 J. Wang, Y. Feng, M. Shi and Y. He, *Sol. Energy Mater. Sol. Cells*, 2024, **275**, 113020, DOI: [10.1016/J.SOLMAT.2024.113020](https://doi.org/10.1016/j.solmat.2024.113020).
- 99 ECHA, Substance Infocard: Lead, <https://echa.europa.eu/es/substance-information/-/substanceinfo/100.028.273>, accessed 18 September 2024.
- 100 S.-Y. Bae, S. Y. Lee, J. Kim, H. N. Umh, J. Jeong, S. Bae, J. Yi, Y. Kim and J. Choi, *Sci. Rep.*, 2019, **9**, 4242, DOI: [10.1038/s41598-018-37229-8](https://doi.org/10.1038/s41598-018-37229-8).
- 101 G. Schileo and G. Grancini, *J. Mater. Chem. C*, 2021, **9**, 67–76, DOI: [10.1039/D0TC04552G](https://doi.org/10.1039/D0TC04552G).
- 102 L. Xu, X. Feng, W. Jia, W. Lv, A. Mei, Y. Zhou, Q. Zhang, R. Chen and W. Huang, *Energy Environ. Sci.*, 2021, **14**, 4292–4317, DOI: [10.1039/D1EE00890K](https://doi.org/10.1039/D1EE00890K).
- 103 ECHA, Substance Infocard: N,N-dimethylformamide, <https://echa.europa.eu/es/substance-information/-/substanceinfo/100.000.617>, accessed 21 January 2025.
- 104 R. Vidal, J.-A. Alberola-Borràs, S. N. Habisreutinger, J.-L. Gimeno-Molina, D. T. Moore, T. H. Schloemer, I. Mora-Seró, J. J. Berry and J. M. Luther, *Nat. Sustain.*, 2020, **4**, 277–285, DOI: [10.1038/s41893-020-00645-8](https://doi.org/10.1038/s41893-020-00645-8).
- 105 J. Sanchez-Diaz, R. S. Sánchez, S. Masi, M. Krečmarová, A. O. Alvarez, E. M. Barea, J. Rodriguez-Romero, V. S. Chirvony, J. F. Sánchez-Royo, J. P. Martinez-Pastor and I. Mora-Seró, *Joule*, 2022, **6**, 861–883, DOI: [10.1016/j.joule.2022.02.014](https://doi.org/10.1016/j.joule.2022.02.014).
- 106 ECHA, Substance Infocard: Ethene, 1,1-difluoro-, homopolymer, [https://echa.europa.eu/es/substance-information/-/substanceinfo/100.133.181#REGULATORY\\_NAMEScontainer](https://echa.europa.eu/es/substance-information/-/substanceinfo/100.133.181#REGULATORY_NAMEScontainer), accessed 24 April 2025.
- 107 CERAFILTEC, PVDF Ban: The Vitally Needed Catalyst for Accelerating Ceramic Membrane Adoption, <https://www.cerafiltec.com/pvdf-ban-the-vitally-needed-catalyst-for-accelerating-ceramic-membrane-adoption/>, accessed 24 April 2025.
- 108 O. E. Solis, M. Mínguez-Avellán, P. F. Betancur, R. I. Sánchez-Alarcón, I. Rodriguez, J. P. Martínez-Pastor, T. S. Ripolles, R. Abargues and P. P. Boix, *ACS Energy Lett.*, 2024, **9**, 5288–5295, DOI: [10.1021/acsenergylett.4C01875](https://doi.org/10.1021/acsenergylett.4C01875).

